AD-A183 138 LOW-SPEED INVESTIGATIONS OF 'APEX FENCE' AND 'CAVITY FLAP' CONCEPTS ON A 6 (U) VIGYAN RESEARCH ASSOCIATES INC HAMPTON VA D M RAO ET AL MAR 87 AFWAL-TR-86-3114 1/1

UNCLASSIFIED F33615-85-C-3008 F/G 20/4 NL

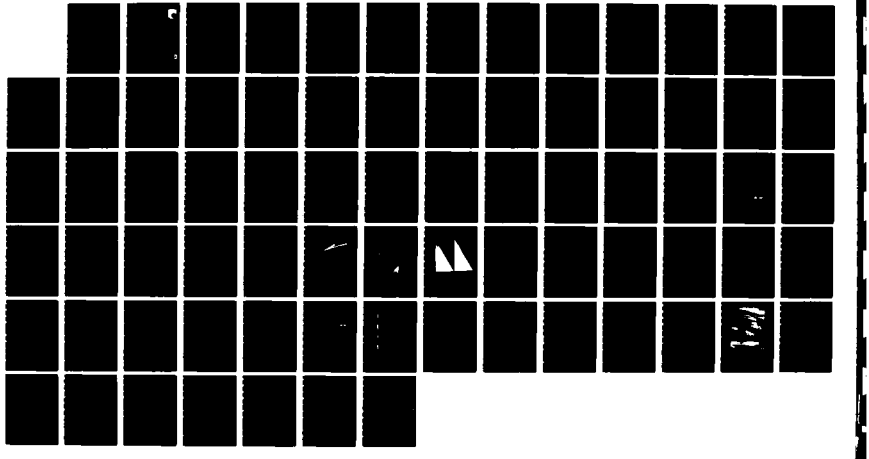

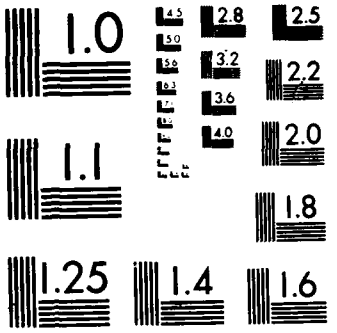

AFWAL-TR-86-3114

LOW-SPEED INVESTIGATIONS OF `APEX FENCE' AND `CAVITY FLAP' CONCEPTS ON A 60 DEGREE DELTA CONFIGURATION

Dhanvada M. Rao
Principal Investigator

Keith D. Hoffler
Associate Investigator

Charles T. L. Mills
Research Engineer

Vigyan Research Associates, Inc.
30 Research Drive
Hampton, VA 23666-1325

March 1987

Final Report for Period March 1985 - October 1986

Flight Dynamic Laboratory
Air Force Wright Aeronautical Laboratories
Air Force Systems Command
Wright-Patterson Air Force Base, OH 45433-6553

NOTICE

When Government drawings, specifications, or other data are used for any purpose other than in connection with a definitely related Government procurement operation, the United States Government thereby incurs no responsibility nor any obligation whatsoever; and the fact that the government may have formulated, furnished, or in any way supplied the said drawings, specifications, or other data, is not to be regarded by implication or otherwise as in any manner licensing the holder or any other person or corporation, or conveying any rights or permission to manufacture use, or sell any patented invention that may in any way be related thereto.

This report has been reviewed by the Office of Public Affairs (ASD/PA) and is releasable to the National Technical Information Service (NTIS). At NTIS, it will be available to the general public, including foreign nations.

This technical report has been reviewed and is approved for publication.

Russell F. Osborn for

Lt Mark C. Frassinelli
Project Engineer
Aerodynamics & Airframe Branch
Aeromechanics Division

Russell F. Osborn for

Bohdan G. Kunciw, Major, USAF
Chief, Aerodynamics & Airframe Branch
Aeromechanics Division

FOR THE COMMANDER

Donald A. Dreesbach, Colonel, USAF
Chief, Aeromechanics Division
Flight Dynamics Laboratory

If your address has changed, if you wish to be removed from our mailing list, or if the addressee is no longer employed by your organization please notify AFWAL/FIMM, *W-PAFB, OH 45433 to help us maintain a current mailing list.*

Copies of this report should not be returned unless return is required by security considerations, contractual obligations, or notice on a specific document.

REPORT DOCUMENTATION PAGE

1a. REPORT SECURITY CLASSIFICATION Unclassified	1b. RESTRICTIVE MARKINGS
2a. SECURITY CLASSIFICATION AUTHORITY	3. DISTRIBUTION/AVAILABILITY OF REPORT Approved for public release; distribution is unlimited.
2b. DECLASSIFICATION/DOWNGRADING SCHEDULE	
4. PERFORMING ORGANIZATION REPORT NUMBER(S)	5. MONITORING ORGANIZATION REPORT NUMBER(S) AFWAL-TR-86-3114
6a. NAME OF PERFORMING ORGANIZATION Vigyan Research Assoc., Inc. 6b. OFFICE SYMBOL (If applicable)	7a. NAME OF MONITORING ORGANIZATION AFWAL/FIMM
6c. ADDRESS (City, State and ZIP Code) 30 Research Drive Hampton, VA 23666-1325	7b. ADDRESS (City, State and ZIP Code) Wright-Patterson AFB, OH 45433-6553
8a. NAME OF FUNDING/SPONSORING ORGANIZATION 8b. OFFICE SYMBOL (If applicable)	9. PROCUREMENT INSTRUMENT IDENTIFICATION NUMBER F33615-85-C-3008
8c. ADDRESS (City, State and ZIP Code)	10. SOURCE OF FUNDING NOS.

PROGRAM ELEMENT NO.	PROJECT NO.	TASK NO.	WORK UNIT NO.
62201F	2404	10	95

11. TITLE (Include Security Classification)
Low-Speed Investigations of 'Apex Fence'

12. PERSONAL AUTHOR(S)
Rao, Dhanvada M.; Hoffler, Keith D.; Mills, Charles T. L.

13a. TYPE OF REPORT	13b. TIME COVERED	14. DATE OF REPORT (Yr., Mo., Day)	15. PAGE COUNT
Final	FROM 3/15/85 TO 10/15/86	87/March	73

16. SUPPLEMENTARY NOTATION

17. COSATI CODES			18. SUBJECT TERMS (Continue on reverse if necessary and identify by block number)
FIELD	GROUP	SUB. GR.	Vortex, Delta Wing, High Lift, Vortex Control High Angle of Attack
01	01	06	
01	01	16	

19. ABSTRACT (Continue on reverse if necessary and identify by block number)

This report describes low-speed wind tunnel investigations of 'apex fence' and 'cavity flap' concepts applied to a 60-deg. uncambered delta wing/body configuration. The upper-surface apex fences, hinged near the leading edges, are deployed vertically at low to moderate angles of attack (appropriate to approach and landing) to force a powerful vortex pair which augments the suction over the forward regions of the wing planform. The resulting nose-up moment is balanced by means of trailing edge flaps, resulting in increased trimmed lift as well as drag for improved short-field landing capability of the tailless delta.

The 'cavity flap' is a lower-surface hinged vortex flap whose deflection creates a frontal cavity underneath the leading edge. Above a certain angle of attack the flap vortex fills the mouth of the cavity, which (a) helps the external flow to turn around the leading edge thus reducing the vortex lift at high angles of attack, and (b) creates suction over the cavity frontal area which generates a side-force component. The potential of asym-

20 DISTRIBUTION/AVAILABILITY OF ABSTRACT	21 ABSTRACT SECURITY CLASSIFICATION
UNCLASSIFIED/UNLIMITED ☒ SAME AS RPT ☐ DTIC USERS ☐	Unclassified

22a NAME OF RESPONSIBLE INDIVIDUAL	22b TELEPHONE NUMBER (Include Area Code)	22c OFFICE SYMBOL
James Grove for Lt. Mark C. Frassinelli	(513) 255-4522	AFWAL/FIMM

11. Title (Continued)

and 'Cavity Flap' Concepts on a 60-Degree Delta Configuration

19. Abstract (Continued)

metrically deployed cavity flaps for lateral/directional control at high angles of attack was of interest.

The above concepts were subjected to low-speed tunnel studies exploring the lee-side flow field through visualizations and pressure surveys, and measuring force and moment characteristics. Pertinent results are discussed which verify the basic aerodynamics of these concepts and assess their potential for trimmed-lift increment and roll/yaw control capability.

ACKNOWLEDGEMENTS

The cooperation and assistance received from tne wind tunnel personnel at North Carolina State University and Air Force Institute of Technology are thankfully acknowledged. The authors also wish to record their gratitude to Lt. Mark C. Frassinelli, contract monitor on behalf of AFWAL, for his active participation and many contributions with respect to the present investigation. The material support provided by AFWAL is thankfully acknowledged.

TABLE OF CONTENTS

LIST OF FIGURES

Figures begin on page 22 and are presented sequentially to page 63.

LIST OF TABLES

SYMBOLS

Coefficients were nondimensionalized by wing area, mean aerodynamic chord, wing span, and/or free stream dynamic pressure as required.

A_R	Fence to wing area ratio (%)
C_L	Lift coefficient
C_{L_T}	Lift coefficient when trimmed with trailing edge flap
C_ℓ	Rolling moment coefficient
C_{ℓ_β}	Derivative of rolling moment with respect to β
C_m	Pitching moment coefficient
C_N	Normal force coefficient
C_n	Yawing moment coefficient
C_{n_β}	Derivative of yawing moment with respect to β
$C_{p,u}$	Upper surface pressure coefficient
$C_{p,l}$	Lower surface pressure coefficient
C_R	Root chord (inches)
d	Distance inboard of leading edge measured perpendicular to the leading edge (inches)
L/D_T	Lift to drag ratio when trimmed with trailing edge flap
x	Distance chordwise measured aft from apex position (inches)
α	Angle of attack measured from wing center plane (degrees)
β	Sideslip angle (degrees)
ΔC_{L_T}	$(C_{L_T}$ FENCE ON $- C_{L_T}$ FENCE OFF$)/C_{L_T}$ FENCE OFF
δ_F	Cavity flap deflection measured from wing center plane perpendicular to the leading edge (degrees)
δ_{FENCE}	Apex fence deflection measured from wing center plane perpendicular to the wing leading edge (degrees)

δ_{TEF}	Trailing edge flap deflection measured from wing center plane perpendicular to hinge line (degrees)
η	Spanwise distance from wing fuselage junction nondimensionalized by the local semispan
Λ	Sweep angle (degrees)

SUBSCRIPTS AND ABBREVIATIONS

H.L.	Hinge line
L.E.	Leading edge
T.E.	Trailing edge

INTRODUCTION

The tailless delta configuration continues to be of interest for supersonic tactical aircraft designs, mainly in view of its low wave drag characteristics. This configuration however is also known to have poor short-field landing performance, due to inadequate longitudinal trim power which precludes the use of trailing edge flaps for low-speed lift augmentation. In addition, the need to share trailing edge controls between pitch and roll functions on a tailless delta restricts longitudinal control capability, particularly in the pitch-down sense for assured recovery from high-alpha maneuvers.

There is considerable interest therefore in investigating novel control concepts generally to improve the low-speed longitudinal controllability, and in particular to provide adequate trim power enabling the use of high-lift trailing edge flaps, without penalizing the inherent high-speed aerodynamic efficiency of the tailless delta configuration. A deployable `apex fence' concept proposed to meet these requirements was subjected to preliminary low-speed wind tunnel investigations, in order to verify the underlying aerodynamics and quantify the longitudinal control potential of the concept across a range of angles of attack on a 60-degree delta.

This report presents a description of the `apex fence' concept and the main results of flow visualizations, wing upper-surface pressure surveys and force/moment measurements performed in two separate wind tunnel test programs. Also included are the results obtained on yet another concept, called the `cavity flap,' investigated for its possible application for lateral/directional control at high angles of attack.

Apex Fence Concept

The lee-side flow field of highly-swept thin delta wings is well known to contain a powerful vortex pair, whose additional suction effect on the wing upper surface contributes substantial lift at moderate to high angles of attack until the occurrence of vortex breakdown. At lower angles of attack appropriate to landing (say $\alpha \leq 10$ degrees) however, the vortex system remains relatively weak and its lift potential limited. The `apex fences' comprise a pair of highly-swept spoiler-like surfaces hinged to the wing upper surface along the forward part of the leading edges (fig. 1).* When raised perpendicularly these fences experience a considerable flow incidence in the lateral plane, consequently generating a powerful counter-rotating vortex pair resembling planar wing vortices corresponding to a much higher angle of attack. The fence vortices create a high level of suction over the wing apex region resulting in a nose-up moment. This moment can be utilized to balance the nose-down moment associated with trailing edge flap deflection, thus augmenting the trimmed lift coefficient of the configuration, at moderate angles of attack. Some early experiments aimed at validating the hypothesized vortex flow characteristics of the apex fences are documented in ref. 1.

Cavity Flap Concept

The `cavity flap' may be described as a lower-surface hinged vortex flap,

---

*Figures and tables are located at end of report.

whose deflection opens a frontal cavity underneath the leading edge (fig. 2). The flap-generated vortex is maintained near the mouth of the cavity, its induced effect assisting the external flow to turn around the wing leading edge. Consequently, leading edge separation is curtailed and the vortex lift contribution reduced. At the same time, vortex suction on the cavity frontal area generates a side force component due to the leading-edge sweep. The vortex lift modulation and lateral force characteristics might be utilized asymmetrically for roll and yaw control functions on a delta wing at high angles of attack when the conventional controls tend to be degraded.

Outline of Investigation

The investigation reported herein was performed in two phases: 1) a preliminary assessment of the fence vortex characteristics and its potential for augmenting the upper-surface suction over the wing apex region, and 2) force and moment tests to evaluate the pitch capability and trimmed-lift increment due to apex fences on a generic model. The wing geometry selected was a 60-degree swept delta with sharp leading edges and symmetric double-diamond airfoil section.

A semi-span model was employed for the initial experiments to facilitate rapid testing of a number of fences, evaluating certain primary variables viz., length, height, shape, hinge-line sweep, hinge-line distance behind leading edge and fence deflection angle. The effect of these variables was observed via flow visualizations and wing upper-surface pressure surveys over an angle-of-attack range. Limited tests were also performed with cavity flaps

on this model.

Follow-up tests were performed with a complete configuration duplicating the semi-span model geometry, measuring six-component forces and moments. The main objective of this phase was to acquire trimmed lift data using apex fences in conjunction with trailing edge flap deflection. The angle-of-attack range was extended to α = 48 deg. Limited oil flow visualizations were also conducted. The force model tests included asymmetric (i.e. deployment on one side only) fence and cavity flap arrangements to evaluate lateral-directional characteristics, as well as sideslip tests with some symmetric fence configurations.

The available documentation on the results of this investigation is listed in references 2 through 6.

MODELS AND TEST DETAILS

Pressure Test

Facility and Instruments: The test was conducted in the North Carolina State University Merrill Subsonic Wind Tunnel. Two Scanivalve pressure transducers with a total capacity of 96 ports were utilized to read 95 of the pressure taps provided on the wing upper surface.

A Sage Action, Inc. Model 3 Helium Bubble Generator was used for flow visualization. A Nikkon F3 camera with a 50-mm lens and polaroid Poloapan 135 film were employed, the latter allowing instant slides to be produced for making the "negative" prints presented herein.

Model: The pressure model was a generic 60-degree semi-span delta wing-body configuration, shaped from 10 lb/ft^3 urethane foam and covered with two layers of 6-oz fiberglass cloth impregnated with polyester resin. A double-diamond symmetrical airfoil section with a thickness ratio of 5.7 percent was employed. The major model dimensions are shown in figure 3.

A total of 100 pressure taps in four spanwise rows on the upper surface were provided on the wing. The locations of 95 connected taps are presented in Table I. The eighth port of the first Scanivalve was bad and hence was omitted from the plots herein.

The fences and cavity flaps were cut from an .040-inch-thick aluminum sheet. Fence deflection angle (measured from the wing center plane) was 90 degrees unless otherwise stated. The six fences investigated and their major dimensions are shown in figure 4. The different fence locations on the wing are shown in figure 5. Cavity flap dimensions and mounting location are shown in figure 6. The complete pressure study test matrix is given in Table II.

The angle of attack measured relative to the wing chord plane ranged from zero to 30 degrees. The pressure tests and helium bubble flow visualization studies were conducted at mean aerodynamic chord Reynolds numbers of 0.06 and 0.11 million, respectively.

Force Test

Facility and Instruments: The test was conducted in the Air Force Institute of Technology 5-foot Subsonic Wind Tunnel. Forces and moments were measured using a six-component strain gauge balance. The sting used had two positions, one for low-alpha and the other for high-alpha range.

Oil flow studies were conducted utilizing a template to obtain a reproducible matrix of oil dots on the wing surface. The model was painted black and the oil was whitened using Titanium Dioxide (TiO_2) to produce a good contrast for the photographs.

Model: The force model was a full-span, 60-deg. delta wing-body configuration, geometrically similar to the pressure model, fitted with a vertical tail (fig. 7). The wing and body were machined from aluminum, and the forebody was wood.

The fences and cavity flaps, were cut from .040-inch-thick aluminum sheets. Twelve fences were tested, their major dimensions are shown in figure 8, and their mounting locations in figure 9. The five cavity flaps are shown in figure 10, and their corresponding mounting positions are shown in figure 11. Tables III and IV contain the complete test matrix for the apex fences and cavity flaps, respectively.

Angle of attack was measured relative to the win centerplane and ranged from -6 deg. to 30 deg. and from 20 deg. to 48 deg. in the low and high alpha sting positions, respectively. The test Reynolds number was 1.11 million based on the wing mean aerodynamic chord.

Additional details of the force and moment investigations and results are documented in references 5 and 6.

RESULTS AND DISCUSSION

Apex Fences

Flow Visualization: Typical helium-bubble photographs taken at α = 10 deg. with a large gothic fence deflected to 75 deg. are presented in fig. 12. With the leading-edge mounted fence, the planar wing vortex is essentially suppressed and the lee-side flow is dominated by the fence vortex. With the fence hinge-line swept at 70 deg., both the leading edge and the fence vortices can be seen. The example presented shows the two vortex cores remaining apart up to the trailing edge, with no apparent tendency of interaction.

The effect of increased angle of attack using the small cropped-delta fence for illustration is shown in fig. 13. At α = 10 deg. the leading edge and fence vortices, while remaining apart, now tend to approach one another with increasing downstream distance, and the fence vortex begins to show signs of breakdown. At α = 20 deg., the two vortices interact strongly and merge, followed by a pronounced breakdown of the merged vortical flow.

Typical upper-surface oil flow patterns obtained on the force model with and without a small gothic fence at α = 9.5 deg. are compared in fig. 14. On the basic wing the leading edge vortex footprint is clearly seen; whereas in the fence-on case the fence vortex dominates the surface flow over most of the wing span, with a sharply reduced leading edge vortex starting aft of the fence.

Overall the flow visualization studies supported the hypothesized vortex generation due to the fence, and indicated that a strong and stable fence vortex could be maintained over most of the wing upper surface at low and moderate angles of attack. A pronounced vortical activity was evident between

the fences, decaying with increasing downstream distance on the wing.

Wing Upper Surface Pressures: A typical set of spanwise pressure distributions showing the effect of gothic fence vortex on the semi-span wing upper-surface flow, representative of the `low-alpha' case (α = 5 deg.), is presented in fig. 15. The stations (A) and (B) which are contained within the fence length show a pronounced increase of the suction level. At the downstream stations (C) and (D), the fence vortex can be distinguished by a local suction peak; and although some modification of the basic wing flow field is indicated, there appears little change in the overall suction level. Essentially similar effects are noted in the case of a delta fence, shown in fig. 16.

At higher angles of attack, represented by the data for α = 20 deg. shown in fig. 17, the fence effect over the wing apex region is opposite of the low-alpha case, i.e. now the suction levels are depressed. Evidently the fence prevents development of high suction peaks from the leading edge vortices as on the basic wing. The average suction over aft stations, however, remains relatively unchanged as in the case of low alpha.

A measure of the local normal force increments on the wing due to fence-induced vortex suction characteristics can be obtained by integrating the upper-surface pressure data. The resulting $C_{N,LOCAL}$ is plotted versus angle of attack for each of the four pressure stations in fig. 18, comparing several fence-on cases with the basic wing. These plots conveniently summarize the typical fence-induced effects over the length of the delta wing: relatively large normal force increments occur over the apex region, with

little change over the aft sections.

Additional fence cases are presented in fig. 19, which also show the typical effect of deflecting the fence to 90 deg. or less from the plane of the wing. The apex-region normal force increment is seen to be effectively controlled by varying the fence angle, indicating the possibility of generating a nose-down moment at high angles of attack by unloading the apex region.

Lift and Pitching Moments: A series of lift and pitching moment characteristics versus angle of attack is presented in figs. 20 to 23, comparing different fence-on cases with the basic wing. The effect of varying fence area is shown for four fence shapes, viz., gothic, delta, cropped delta, and double gothic. In general, the fences produce a lift increment together with a nose-up moment increment relative to the basic wing characteristics, increasingly with increasing fence area. These effects are consistent with the upper-surface pressure measurements already discussed. It is worth noting that the nose-up moment increments remain practically constant up to nearly 20 degrees angles of attack. At higher alphas, the moment increments consistently show a downtrend, whose extrapolation would lead one to expect nose-down moments above α = 30 deg. (depending on the fence area and shape).

The effect of moving the fence hinge line parallel to and inboard of the leading edge, for the cropped fence, is shown in fig. 24. A progressive reduction in pitching moment increment is indicated with increasing hinge-line distance (d) from the leading edge, although the effect on lift curve is negligible. A small distance (in relation to fence height) from the leading

edge seems permissible for structural reasons without seriously degrading the fence effectiveness.

Variation in the fence angle from a nominal 90-deg. position indicates potential for pitching moment control, as shown in fig. 25 for the double-gothic fence. A relatively large and smooth change in the pitching-moment increment for only a small variation in fence angle on either side of Λ_{FENCE} = 90 deg. is obtained.

The effect of trailing edge flap deflection on the basic model is shown in fig. 26. The resulting nose-down moments can be seen to be of the same order as the nose-up moments due to apex fences on this configuration. Thus, simultaneous fence deployment and trailing edge flap deflection will provide substantial trimmed-lift increments, over a broad angle-of-attack range.

All fence configurations were not tested in conjunction with trailing edge flaps. Therefore, using the lift and pitching moment increments produced by trailing-edge-flap deflection on the planar wing, trimmed lift coefficients for the planar wing and fence-deployed configurations at a specified angle of attack (= 12 deg.) were calculated of the purpose of comparing the various fence configurations. These results are presented as a bar chart in fig. 27. The first bar indicates the lift coefficient of basic model using up-deflected trailing edge flaps for trim. Other bars indicating the C_{L_T} at the same angle of attack obtained by the use of fences are grouped according to the fence-shape family and in the order of decreasing fence to wing area ratio in each group. The general effect of reducing fence area is to decrease C_{L_T}, regardless of the fence shape.

In an attempt to separate out the fence-shape effect, if any, from

fence-area effect the percentage increment of C_{L_T} (at α = 12 deg.) has been plotted versus fence area as a percentage of the wing area in fig. 28. This plot generally shows the C_{L_T} to increase in proportion to the fence area, with only the double-gothic fence having a concave-tapered-trailing-edge standing out as the `best' shape. Although no conclusions can be based on the single data point available for this shape, a detailed investigation of this fence geometry with respect to its area efficiency seems warranted.

The high suction level observed on the wing apex region would also be expected to act on the inside of the fence surfaces, generating a sizeable drag increment. The L/D_T characteristics comparing fence-on and fence-off cases in fig. 29 indicate the considerable fence drag incurred. Controlled drag capability is desirable as a means of reducing the touch-down speed of modern fighters, which approach and land with a relatively high engine thrust setting. The drag generated by apex fences can be readily controlled by varying the fence deflection; the associated flow field being vortex-stabilized should produce a low buffet level.

It was observed in the pressure results that at high angles of attack the fence effect on the wing apex was opposite to the low-alpha case, viz., a reduction of the suction level compared to the planar case. This is borne out by the lift and pitching moment measurements in the range 23 deg. $< \alpha <$ 45 deg. shown in fig. 30. The results are for the gothic fences and typical of all the fences investigated, indicating the potential of fence deployment to accelerate recovery from high-alpha maneuvers.

An example of apex fence asymmetric deployment, i.e., with only the left

fence on, is presented in fig. 31. The asymmetric fence would be expected to generate useful lateral/directional control moments. The side force on the left fence produces a nose-right yawing moment over most of the angle-of-attack range. However, the accompanying rolling moment is adverse, i.e. left wing down between α = 5 deg. and 20 deg. In this range, an inboard shift of the center-of-lift on left wing panel appears to be the dominant effect of the fence vortex. From the observed trends, the asymmetric fence may be more useful for roll control at higher angles of attack.

The directional and lateral stability characteristics with a pair of gothic fences deployed symmetrically are presented in fig. 32. Note that the basic delta wing becomes unstable at angles of attack above 25 degrees with fences off. Both lateral and directional stability are improved with the fences deployed. The data shown was derived from sideslip angles of $\pm$ 3 deg.; the fence effect on lateral/directional characteristics at high sideslip angles needs investigation.

Cavity Flaps

Flow Visualization: Oil flow studies were conducted on the force model with some of the cavity flap configurations. The main purpose was to confirm the presence of a steady vortex flow inside the flap/wing cavity. Selected oil-flow photographs highlighting the patterns on the upper surface of the cavity flap mounted under the left wing panel are presented in fig. 33. The two photos at the top are for a cavity flap hinged along the root chord, at angles of attack 9.5 deg. and 20 deg. In both cases a vortex can be

inferred to exist in the cavity, as indicated by the outflow of oil streaks until they merge into a common ray representing secondary separation. The oil patterns indicate that the cavity vortex is enlarged and strengthened with increasing angle of attack. The bottom photo is for the case of cavity flap hinge line swept at 70 deg. at α = 20 deg., which also indicates a well-defined vortex flow pattern on the flap upper surface.

Wing Surface Pressures: The effect of a cavity flap can be observed in the wing upper and lower surface pressures at the first two stations, i.e., A and B, presented in fig. 34 (the aft stations C and D showed little change from the basic wing pressures and were omitted from the figure). At α = 10 degrees the spanwise $C_{p,L}$ distributions are relatively unchanged across the hinge line, indicating the absence of a cavity vortex (or perhaps a very small vortex on the flap surface whose influence does not extend across the cavity to the wing surface). The corresponding upper-surface pressures on the wing also are essentially unaltered. At α = 15 degrees, however, the spanwise $C_{p,L}$ jumps discontinuously across the hinge line to negative values indicating the presence of a substantial cavity vortex (fig. 35). In this case, the wing upper surface suction at station A is significantly reduced in the leading edge region, indicating a diminished apex vortex.

Force and Moment: The primary interest in applying the cavity flap concept in the present study was to generate yaw and roll control at high angles of attack when the conventional rudder and aileron surfaces begin to lose their effectiveness. Thus, the yawing and rolling moment capability of asymmetric cavity flaps would be the main focus of this discussion. However,

one case of symmetrically-deflected cavity flaps is considered, in view of the foregoing pressure measurements. The lift and pitching moment characteristics presented in fig. 36 show that while the effect on lift is negligible, a significant nose-down increment in the pitching moment appears starting at α = 15 deg. This effect is consistent with the reduced suction observed over the wing apex region when a vortex is captured in the flap cavity. These results are indicative of the cavity flap potential in controlling the vortex characteristics of a delta wing. This nose down increment is maintained to α = 40 deg. where the cavity flap begins to produce a nose up increment (fig. 34). This is believed to be the effect of flap vortex spilling from the cavity on to the wing upper surface.

The high-alpha rolling moment and yawing moment characteristics with an asymmetric cavity flap (i.e. deployed on the left side only), at two alternate positions, i.e. hinged at root-chord and along a 70 deg. swept ray, at a constant deflection of 60 degrees, are compared with the basic wing in fig. 38. Both the cavity flaps show a substantial left-wing-down rolling moment, which is consistent with a reduced vortex lift over the left wing panel, i.e., the side on which the cavity flap is deployed. The rolling moment is also accompanied with an adverse yawing moment over a part of the alpha range. Between the two flap positions considered, the 70 deg. swept hinge line generates considerably higher roll power as well as a minimum of adverse yaw.

A set of results at varying flap deflection angle from 30 deg. to 75 deg. is presented in fig. 39. The flap angle is found to have relatively little effect on the rolling and yawing moment characteristics; therefore, this type of cavity flap appears unsuitable as a proportional control surface.

A third flap position representing the other extreme, i.e., hinged along

the leading edge, was also investigated. In this case, the deployed flap would rotate outwards forming a reversed cavity. The results in fig. 40 show that this type of flap produces high-alpha rolling and yawing moment characteristics quite similar to the flaps previously discussed; however the roll power appears somewhat more responsive to flap angle.

In the results pertaining to cavity flap effects at high angles of attack, it is observed that the flap-on rolling and yawing moment characteristics appear remarkably as mirror images of the basic model (flap off) characteristics. The basic model develops lateral/directional moments following the onset of asymmetry in the forebody vortex shedding, which in the present case occurs at $\alpha \sim 30$ degrees. Thus, it is possible that the cavity flap essentially fixes the orientation of baseline asymmetry, rather than generating a distinctive flow field of its own. The relatively weak effect of flap angle variation tends to support this possibility. In order to obtain definitive results characterizing the cavity flap concept, therefore, a baseline configuration having relatively innocuous high-alpha asymmetry characteristics may have to be employed.

CONCLUDING REMARKS

Apex Fences

Flow visualization and upper-surface pressure surveys on the delta wing have verified the basic premise of this concept, viz., of forcing a powerful, stable vortex pair at low to moderate angles of attack which considerably enhances the suction level over the wing apex region. Force and moment measurements show that this results in a nose-up moment which, when trimmed with trailing edge flaps, yields a considerable increase in the usable lift

coefficient plus a drag increase, both of which can be utilized to improve the short-field landing capability of tailless delta configurations. At high angles of attack, fence deployment permits partial unloading of the wing apex region, thus generating a nose-down moment useful for acclerated recovery from a high-alpha maneuver while fence angle variation provides a smooth pitch control. Asymmetric (i.e. one sided) fence deployment generates a yawing moment with adverse induced roll. Symmetrically deployed fences improve the directional/lateral stability at small sideslip angles.

Cavity Flap

The objective here was to explore the lateral/directional control potential at high angles of attack. Although substantial rolling moments were generated by deploying asymmetric cavity flaps, these occurred in the alpha range where the baseline configuration itself was dominated by asymmetries induced by forebody vortex shedding. The present results suggest the possibility that one-sided flap deployment altered the flow on that wing panel just enough to switch the orientation of the baseline asymmetry. From this highly interactive flow, it is not feasible to extract the cavity flap characteristics per se. Accordingly, any further investigation of the cavity flap concept, and any high-alpha lateral/directional aerodynamic control concept, should be performed on a baseline configuration which has relatively innocuous nigh-alpha asymmetry characteristics.

REFERENCES

1. Wahls, R. A., Vess, R. J., and Moskovitz, C. A., "Experimental Investigation of Apex Fence Flaps on Delta Wings," J. Aircraft, Vol. 23, No. 10, October 1986.

2. Rao, D. M. and Hoffler, K. D., "Pressure and Flow Studies of Vortex Fences and Cavity Flaps on a 60-Deg. Delta Wing," Interim Report Submitted to AFWAL (FIMM),

3. Hoffler, K. D., Rao, D. M. and Frassinelli, M. C., "Basic Studies on Delta Wing Flow Modifications by Means of Apex Fences," NASA CP-2416, October 1985.

4. Hoffler, K. D., Rao, D. M., and Frassinelli, M. C., "Low-Speed Aerodynamics of Apex Fences on a Tailless Delta Configuration," AIAA Paper No. 1838-CP, June 1986.

5. Smith, H. C., "Experimental Assessment of Vortex Retaining Cavity Flaps for Maneuverability Improvement on Delta Wing Fighter Aircraft," AFIT/GAE/AA/85D-13, M.S. Thesis, Air Force Institute of Technology Wright-Patterson AFB, December 1985.

6. Stuart, M., "Experimental Study of Apex Fences for Lift Enhancement on a Highly Swept Delta Wing Configuration," AFIT/GAE/AA/85D-14, M. S. Thesis, Air Force Institute of Technology, Wright-Patterson AFB, December 1985.

TABLE I

PRESSURE TAP LOCATIONS

STATION 1 $X/C_R = 0.2$		STATION 2 $X/C_R = 0.4$		STATION 3 $X/C_R = 0.6$		STATION 4 $X/C_R = 0.8$	
TAP	2Y/B	TAP	2Y/B	TAP	2Y/B	TAP	2Y/B
1	0.124	18	0.079	41	0.052	68	0.033
2	0.180	19	0.117	42	0.084	69	0.061
3	0.224	20	0.158	43	0.118	70	0.092
4	0.276	21	0.196	44	0.151	71	0.126
5	0.320	22	0.231	45	0.185	72	0.157
6	0.372	23	0.269	46	0.218	73	0.190
7	0.432	24	0.342	47	0.251	74	0.222
8	0.485	25	0.377	48	0.286	75	0.253
9	0.532	26	0.415	49	0.319	76	0.285
10	0.580	27	0.451	50	0.353	77	0.316
11	0.632	28	0.488	51	0.386	78	0.349
12	0.684	29	0.526	52	0.418	79	0.381
13	0.732	30	0.563	53	0.453	80	0.445
14	0.780	31	0.613	54	0.487	81	0.477
15	0.832	32	0.638	55	0.555	82	0.509
16	0.880	33	0.680	56	0.588	83	0.542
17	0.940	34	0.713	57	0.623	84	0.574
		35	0.761	58	0.657	85	0.606
		36	0.787	59	0.690	86	0.638
		37	0.824	60	0.723	87	0.672
		38	0.862	61	0.756	88	0.703
		39	0.897	62	0.788	89	0.735
		40	0.935	63	0.822	90	0.801
				64	0.854	91	0.833
				65	0.899	92	0.865
				66	0.922	93	0.896
				67	0.949	94	0.927
						95	0.955

TABLE II

PRESSURE TEST SUMMARY

TEST NUM.	CONFIGURATION
1	PLANAR WING
2	BASELINE FENCE
3	CROPPED 1
4	CROPPED 1 - PARALLEL TO LEADING EDGE
5	CROPPED 2
6	GOTHIC
7	CROPPED 2 - SWEPT 70°
9	GOTHIC - δ_F = 75°
10	DELTA
11	GOTHIC - δ_F = 58°
12	DOUBLE GOTHIC
13	GOTHIC - SWEPT 70°, δ_F = 75°
14	GOTHIC - SWEPT 70°
15	CROPPED 2 - PARALLEL TO LEADING EDGE
16	CAVITY FLAP (LOWER SURFACE MEASUREMENTS)
17	CAVITY FLAP (UPPER SURFACE MEASUREMENTS)

(UNLESS OTHERWISE NOTED, FENCES ARE MOUNTED ALONG LEADING EDGE AND δ_F = 90°)

TABLE III

APEX FENCE FORCE TEST SUMMARY

FENCE	δ_F	d	α RANGE		SYMMETRY		SIDE SLIP
			LOW	HIGH	SYMM	ASYMM	
AF-1	75	0	x		x		
	90	0	x	x	x		x*
AF-2	90	$\pm$ 0	x	x	x		
AF-3	90	0	x	x	x	x*	
AF-4	75	$\pm$ 0	x	x	x	x	
	90	0	x	x	x		
AF-5	90	0	x	x	x		
AF-6	90	0	x	x	x		
AF-7	90	$\pm$ 0	x	x	x		
AF-8	90	0	x	x	x		
AF-9	90	0	x	x	x		
AF-10	90	0	x	x	x		
AF-11	75	0	x	x	x		
	82.5	0	x	x	x		
	90	$\pm$ 0	x	x	x	x	
	97.5	0	x	x	x		
AF-12	90	0	x	x	x		

*Low α Only

TABLE IV

CAVITY FLAP FORCE TEST SUMMARY

FLAP/POSITION	δ_F	α RANGE		SYMMETRY		SIDE SLIP
		LOW	HIGH	SYMM	ASYMM	
CF-1/P6	90	x			x	
CF-2/P3	75	x			x	
	60	x			x	
CF-3/P1	30	x	x	x	x	x
	45	x	x	x	x	
	60	x	x	x	x	x
	75	x	x		x	
CF-3/P2	45	x	x	x	x	
	60	x	x	x	x	
CF-3/P3	30	x	x	x	x	
	60	x	x	x	x	
	90	x	x	x	x	
CF-3/P4	90	x	x		x	
CF-3/P6	90	x	x		x	
CF-3/P7	60		x		x	
CF-4/P2	30	x	x	x	x	
	45	x	x		x	
	60	x	x	x	x	
	75	x	x		x	

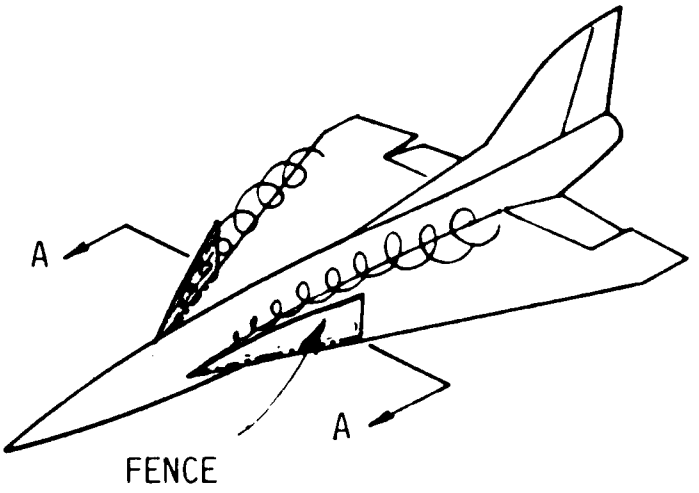

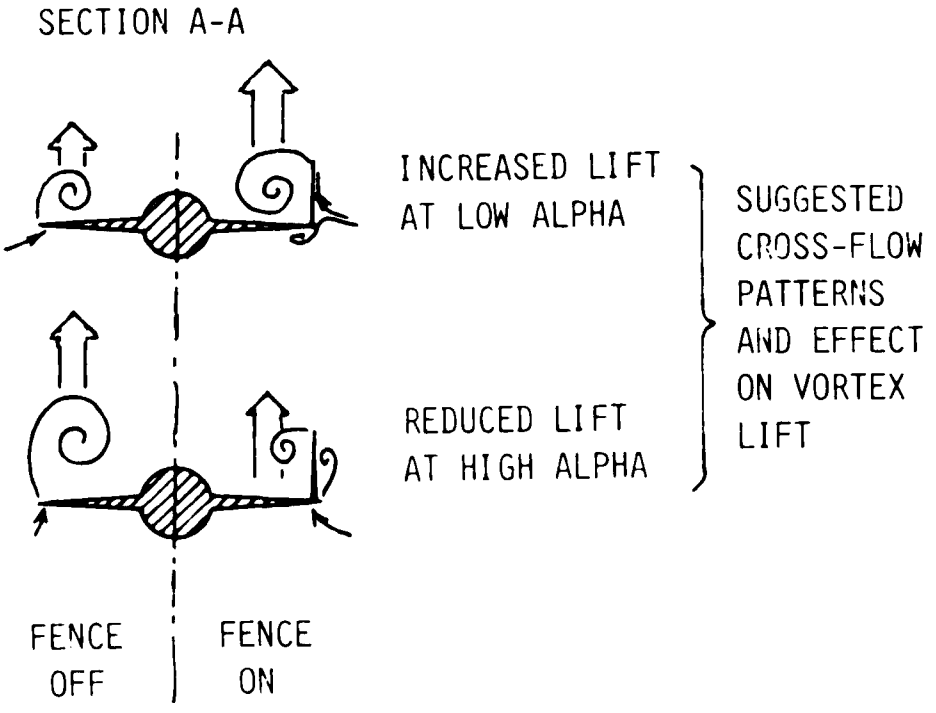

Fig. 1. Apex Fence Concept

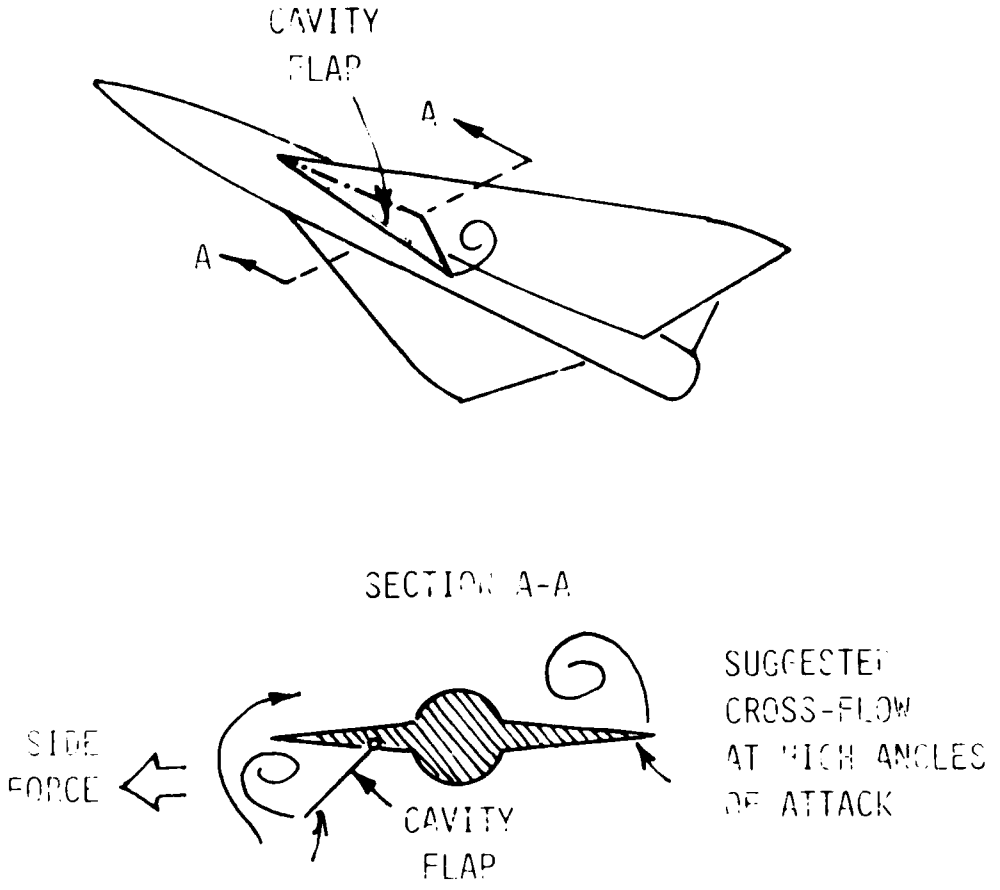

Fig. 2. Cavity Flap Concept

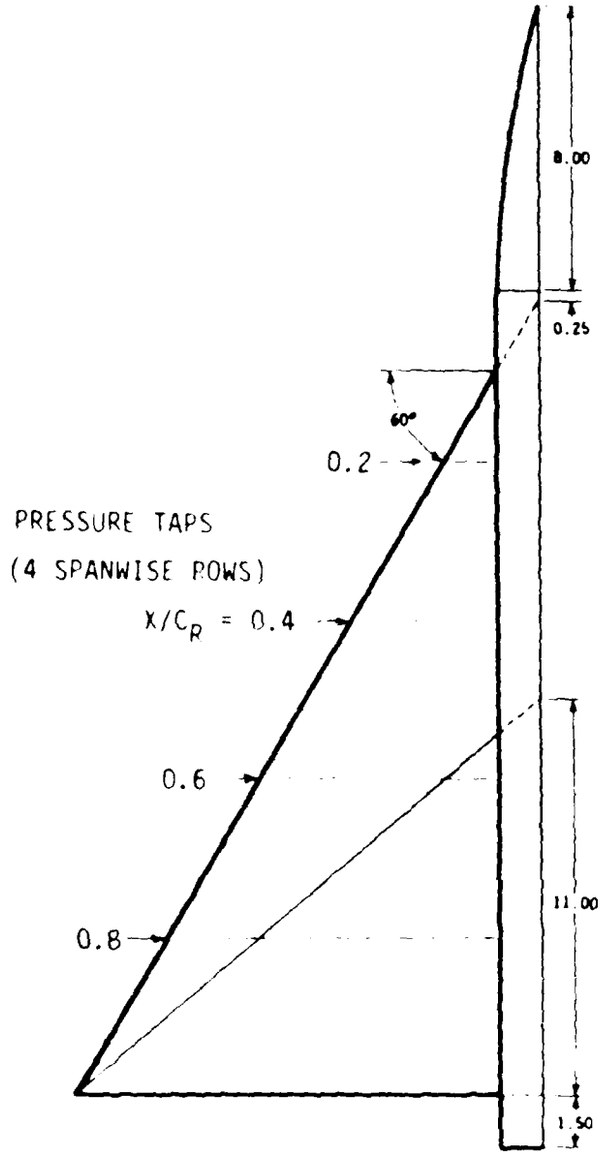

ROOT SECTION

Fig. 3. Semi-span pressure model. Dimensions in inches.

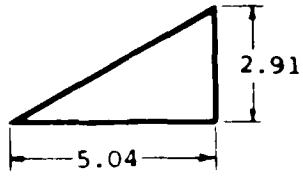

BASELINE

5.2 %

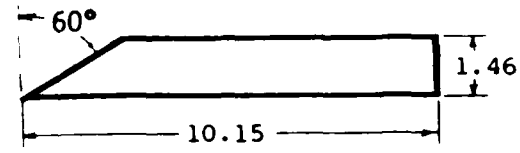

CROPPED 2

9.3 %

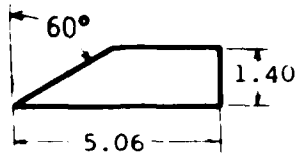

CROPPED 1

3.8 %

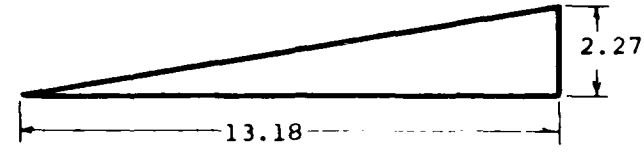

DELTA

10.6 %

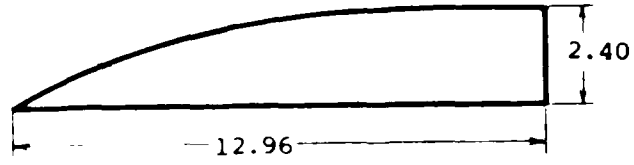

GOTHIC

16.7 %

A_R

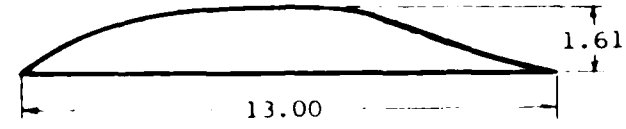

DOUBLE GOTHIC

10.2 %

Fig. 4. Geometry of fences tested on pressure model. Dimensions in inches.

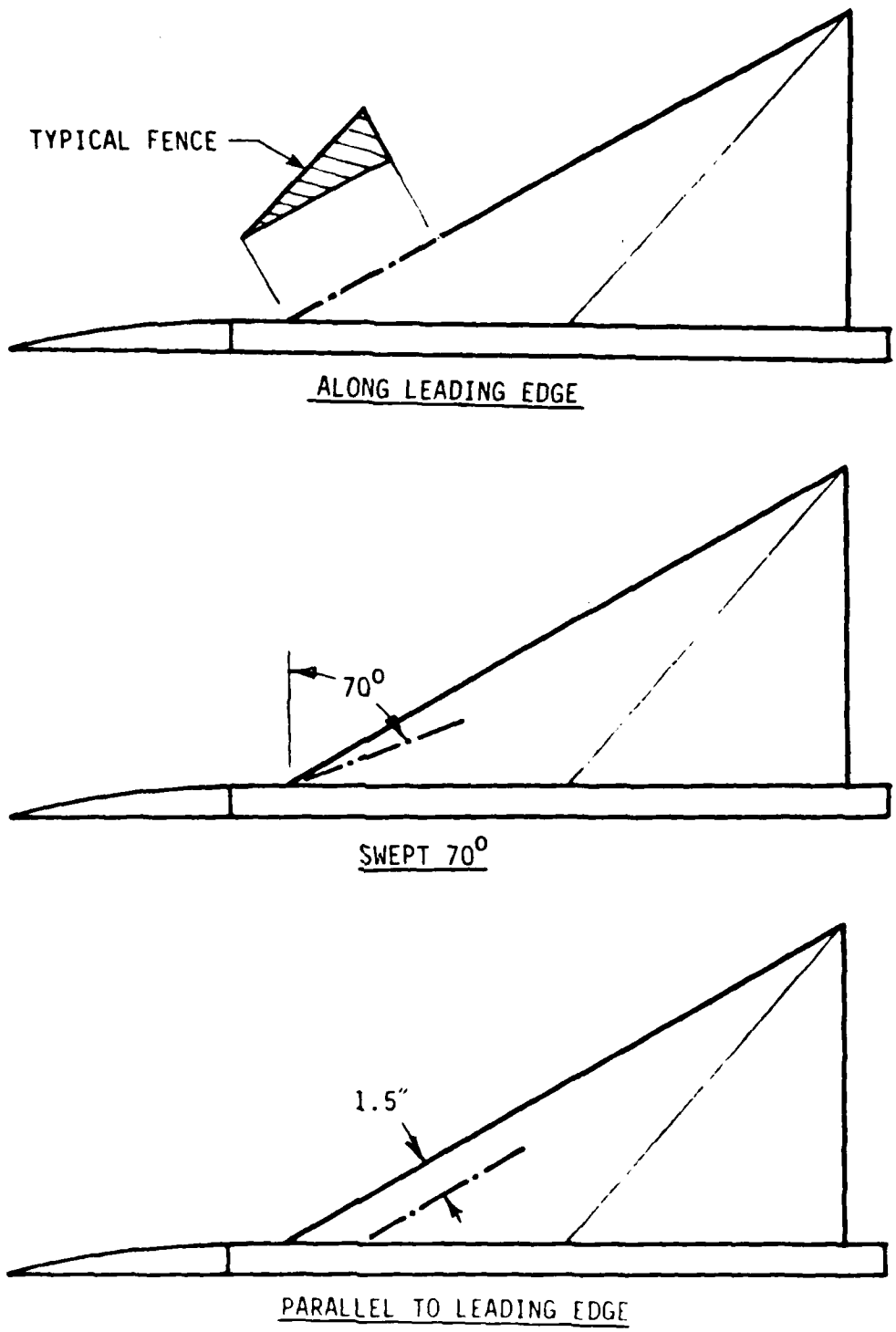

Fig. 5. Fence locations on the pressure wing.

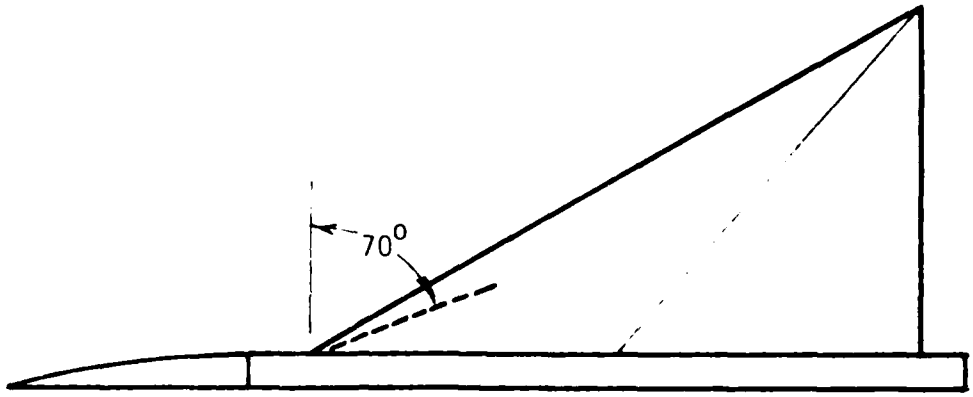

MOUNTED ON LOWER SURFACE; SWEPT 70°

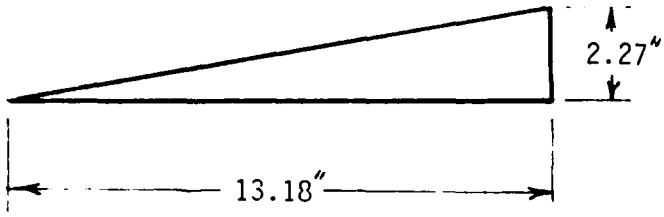

A_R = 10.6

Fig. 6. Cavity flap geometry and locations on the pressure wing.

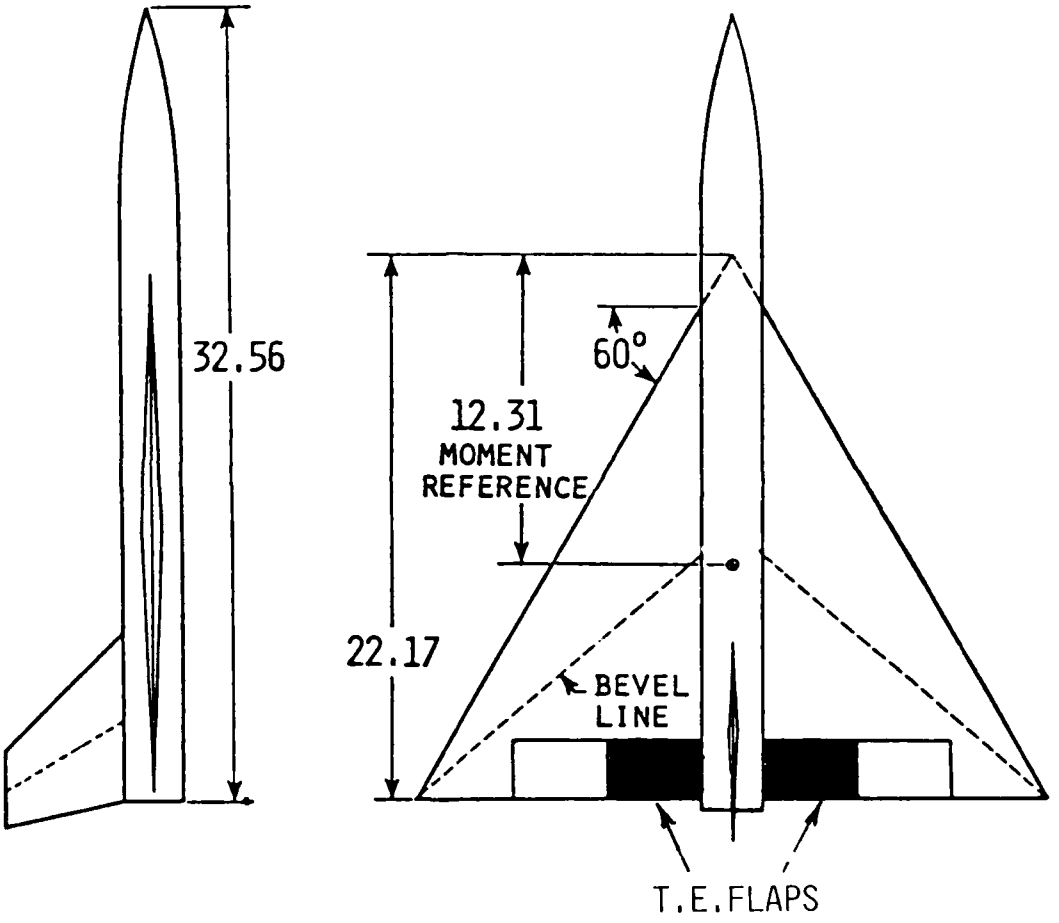

Fig. 7. Force/moment test model.

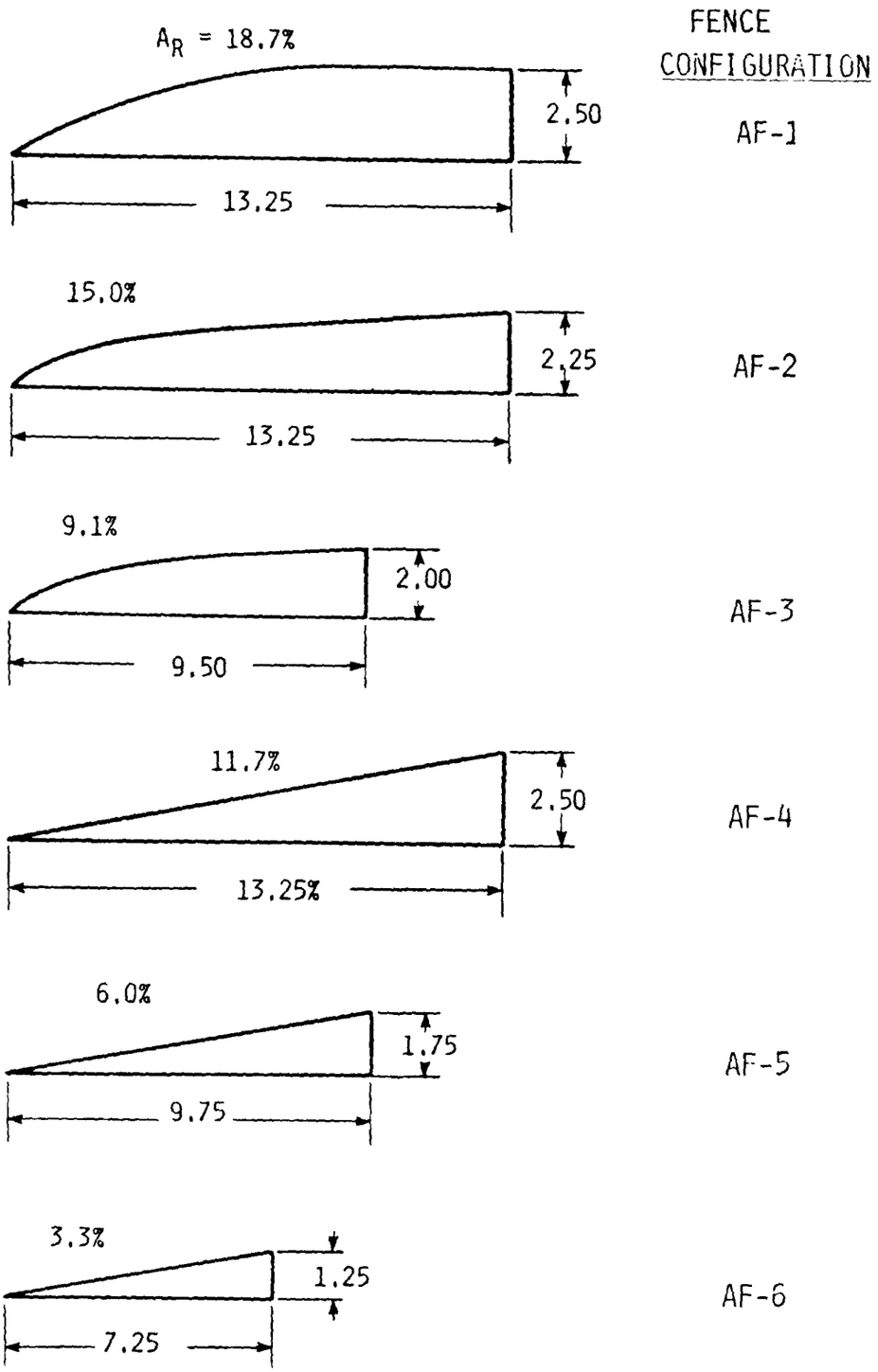

Fig. 8. Force model fences. Dimensions in inches. (Continued).

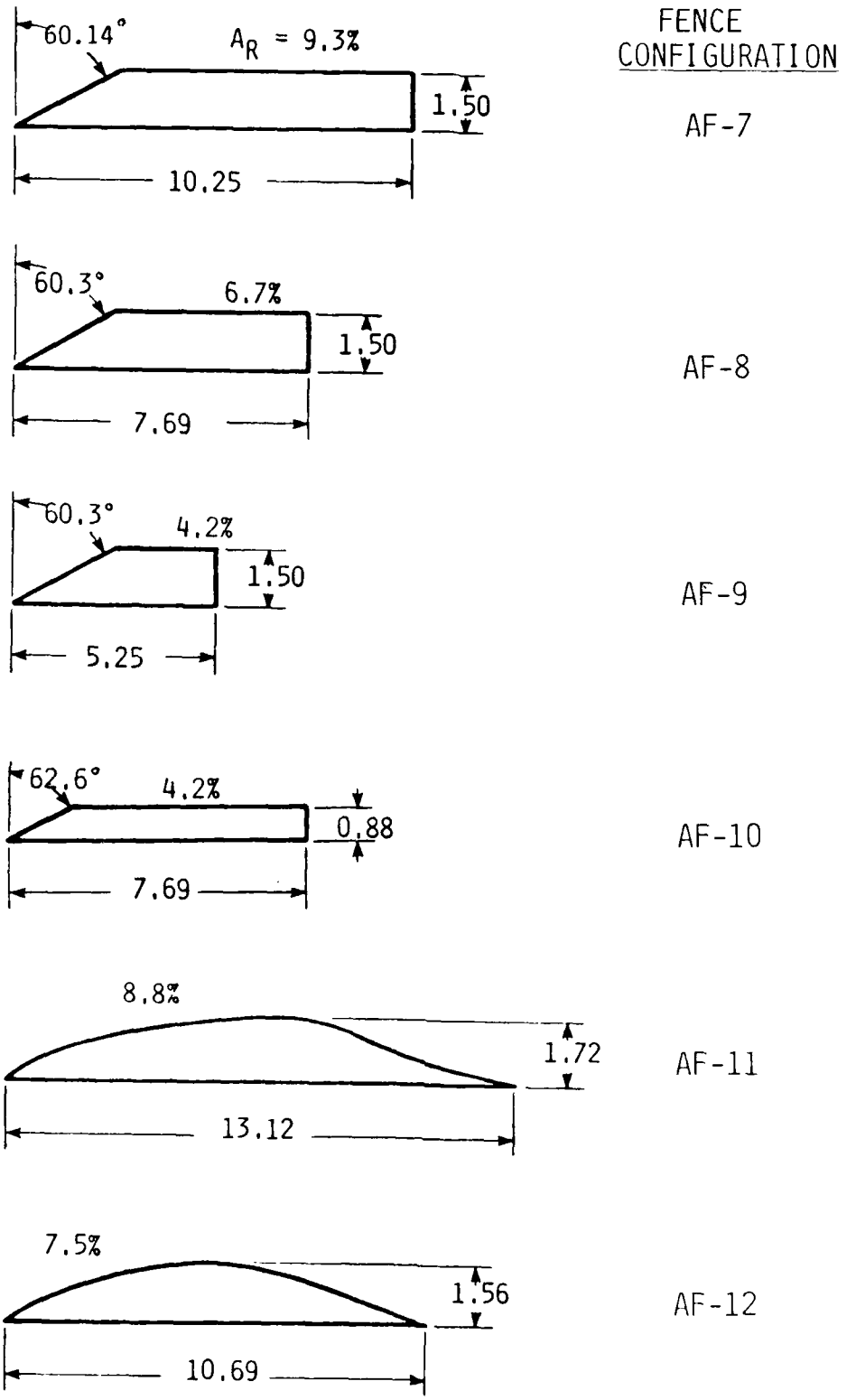

Fig. 8. Concluded.

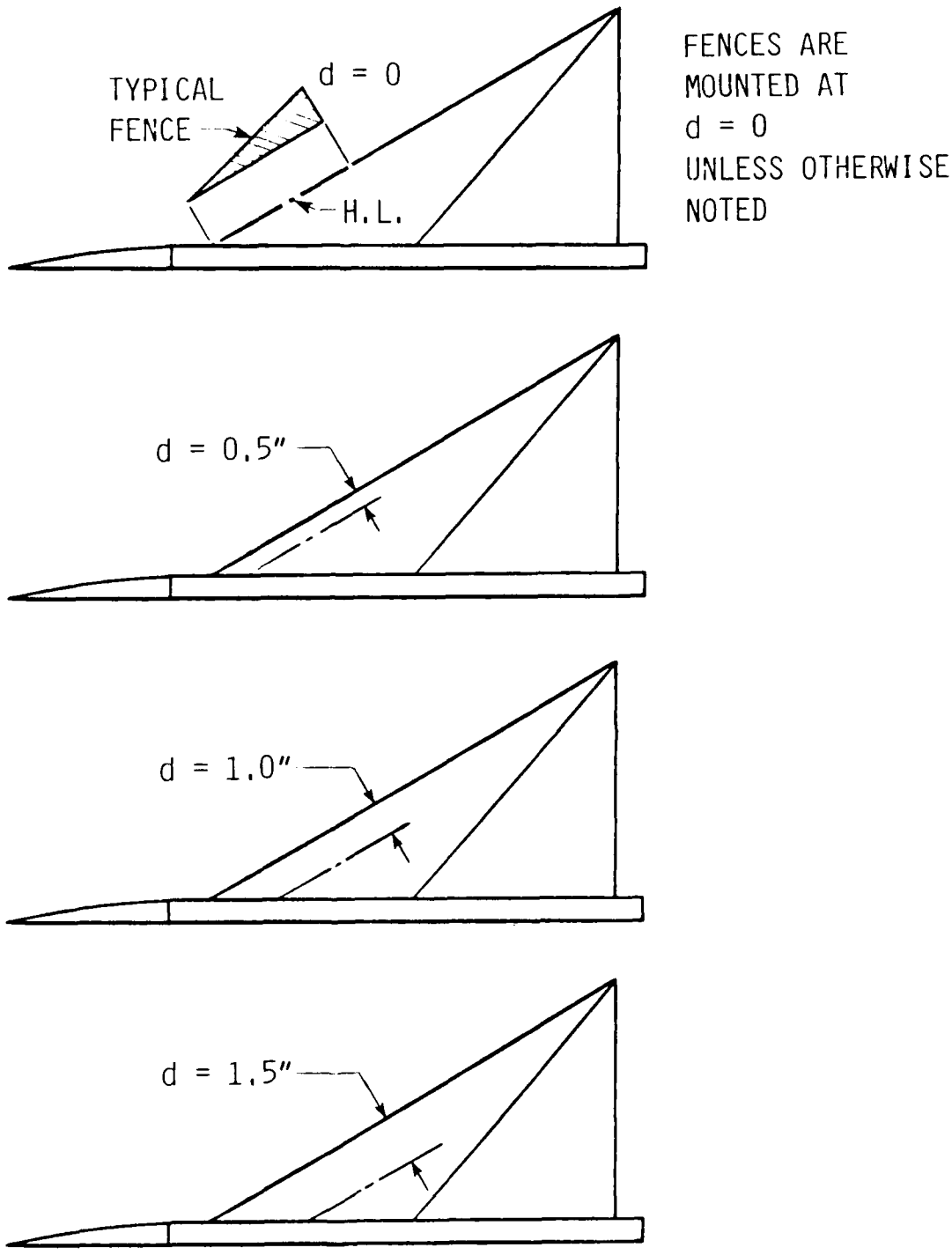

Fig. 9. Fence locations on force model.

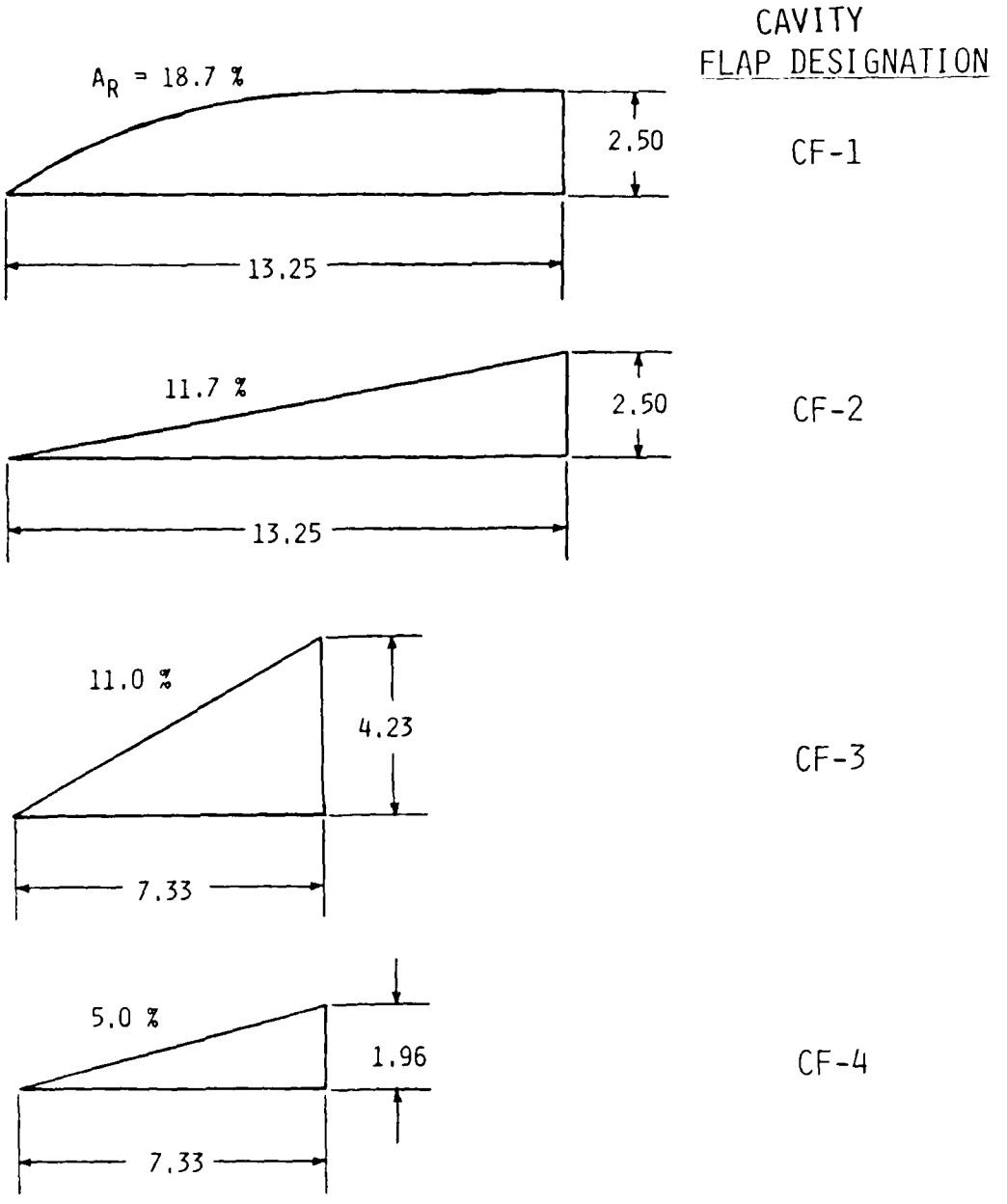

Fig. 10. Force model cavity flaps. Dimensions in inches.

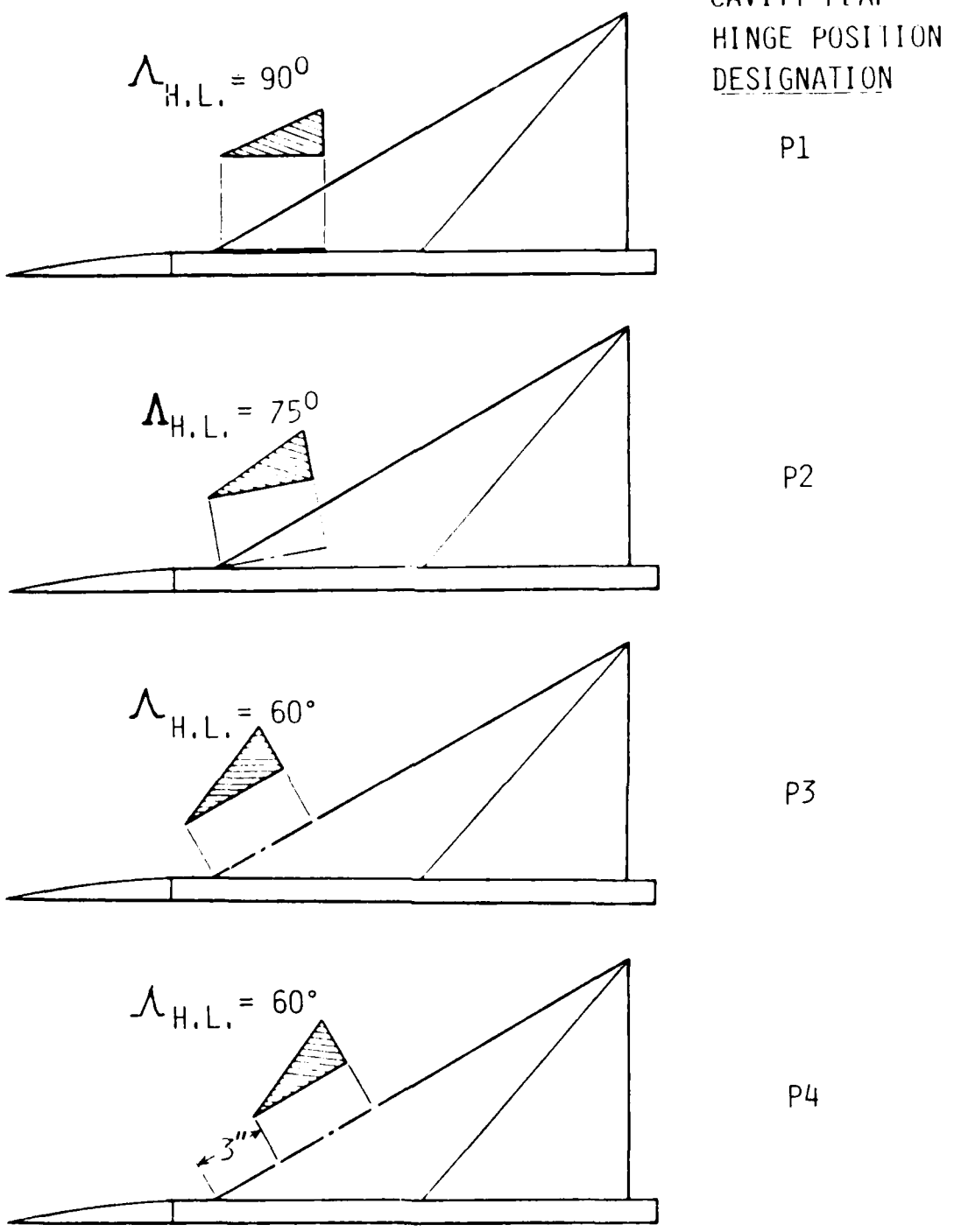

Fig. 11. Cavity flap positions on force model. (Continued).

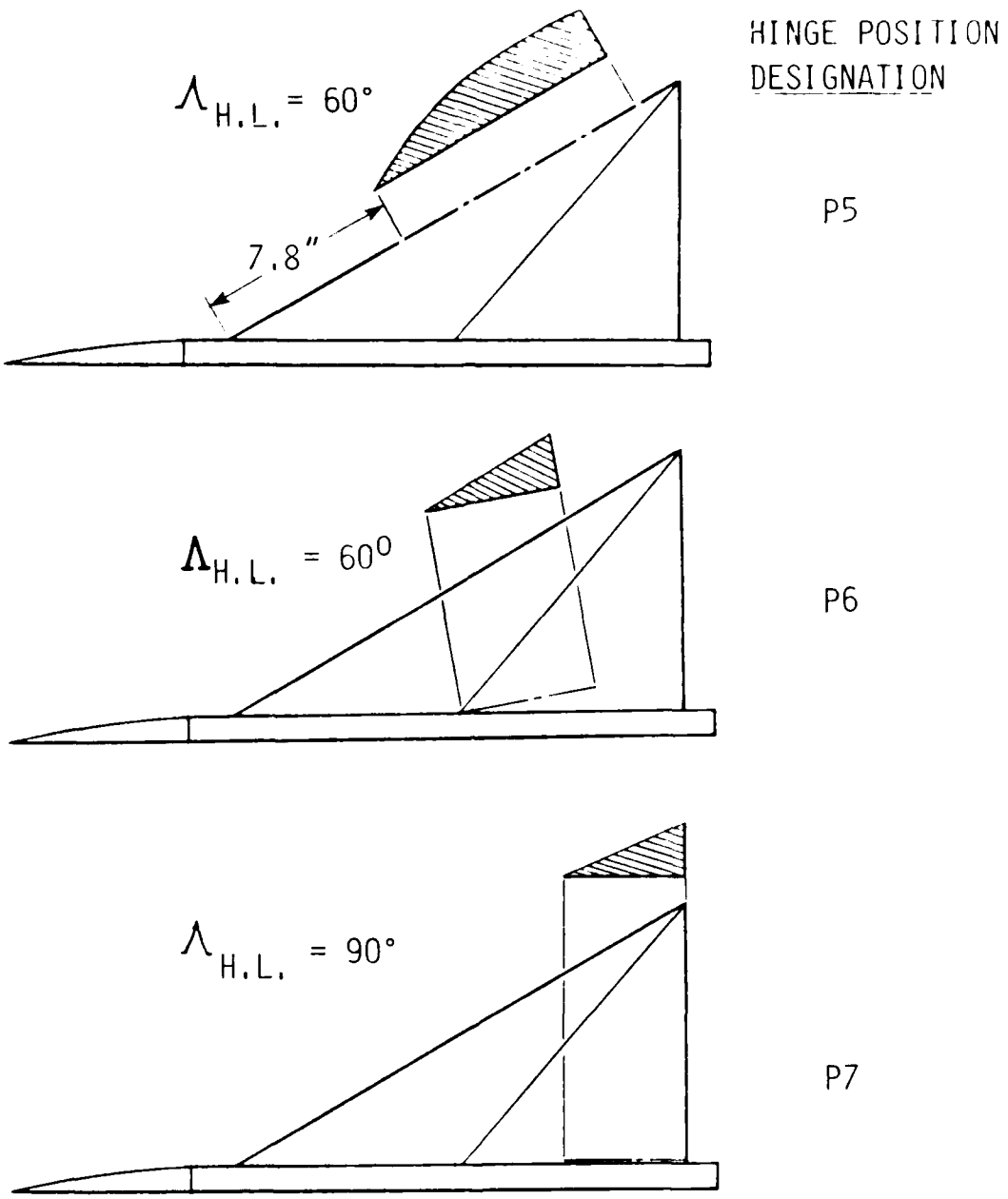

Fig. 11. Concluded.

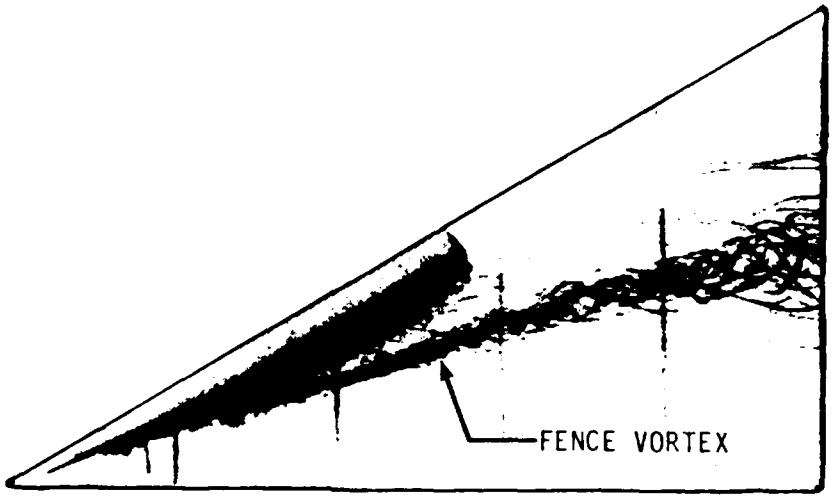

FENCE ALONG L.E.

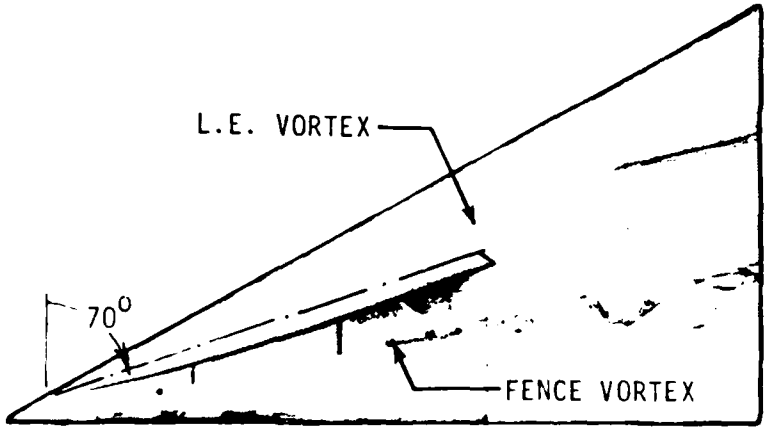

FENCE SWEPT 70°

Fig. 12. Helium bubble visualization on pressure model at 10 degrees angle of attack, showing effect of fence location on vortex characteristics.

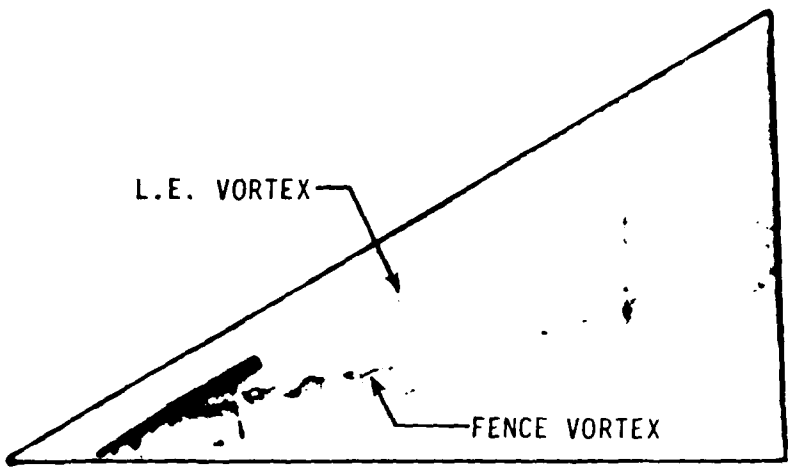

$\alpha = 10^{o}$

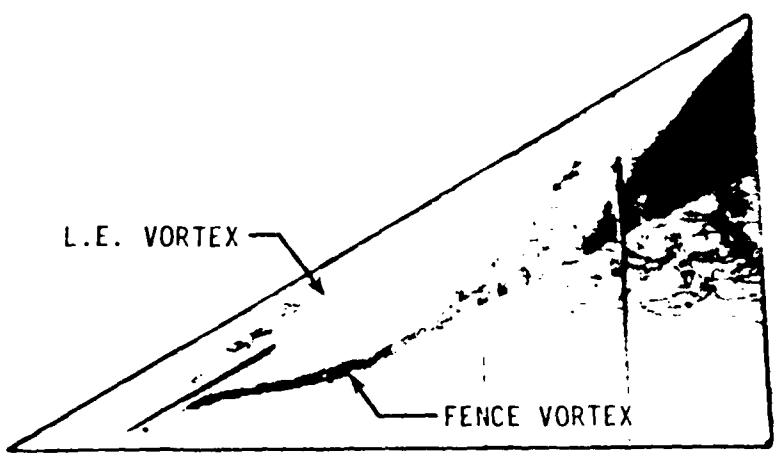

$\alpha = 20^{o}$

Fig. 13. Helium bubble visualization on pressure model, showing angle-of-attack effect on fence vortex characteristics

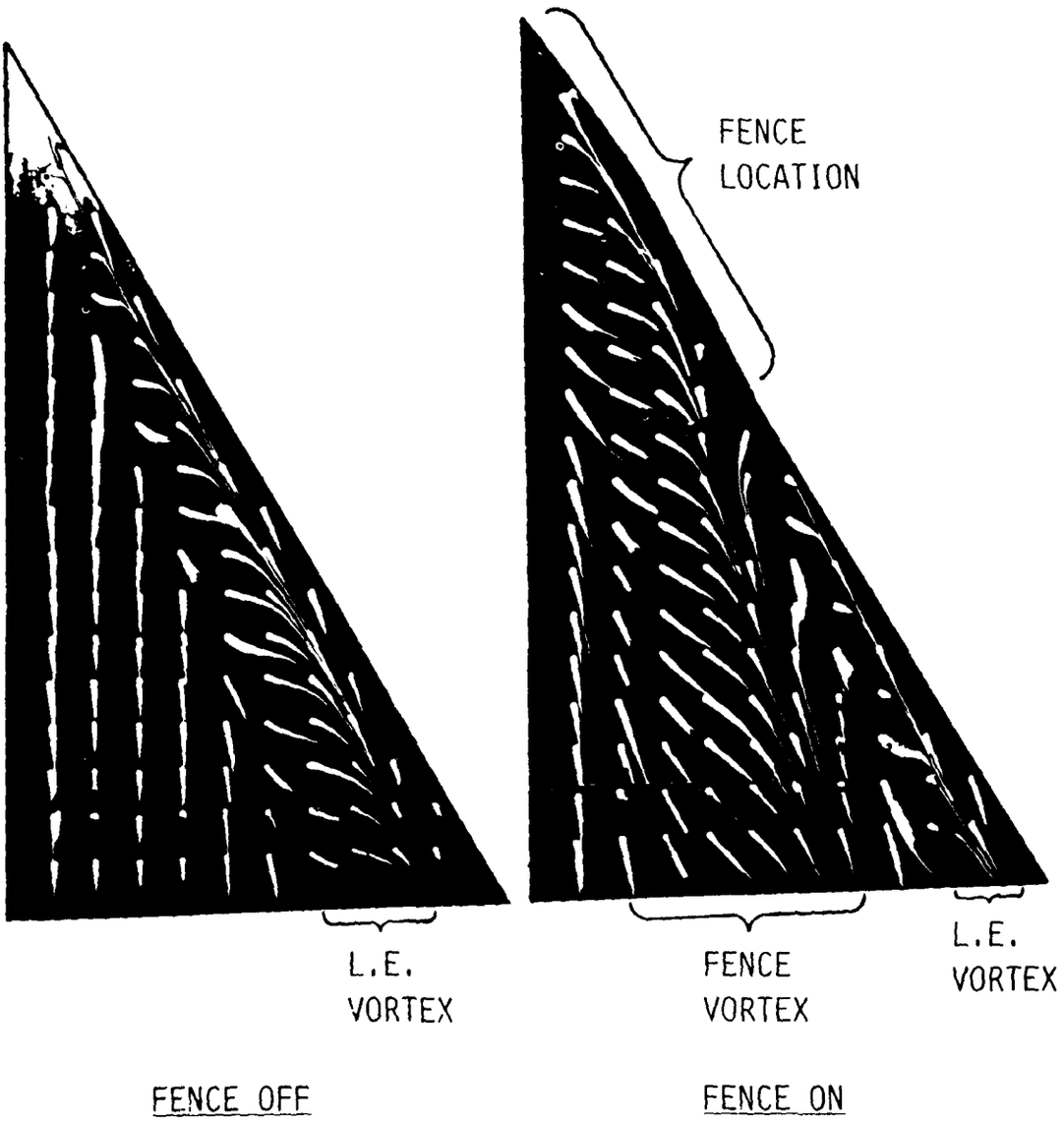

Fig. 14. Oil flow visualization on force model with and without fences.

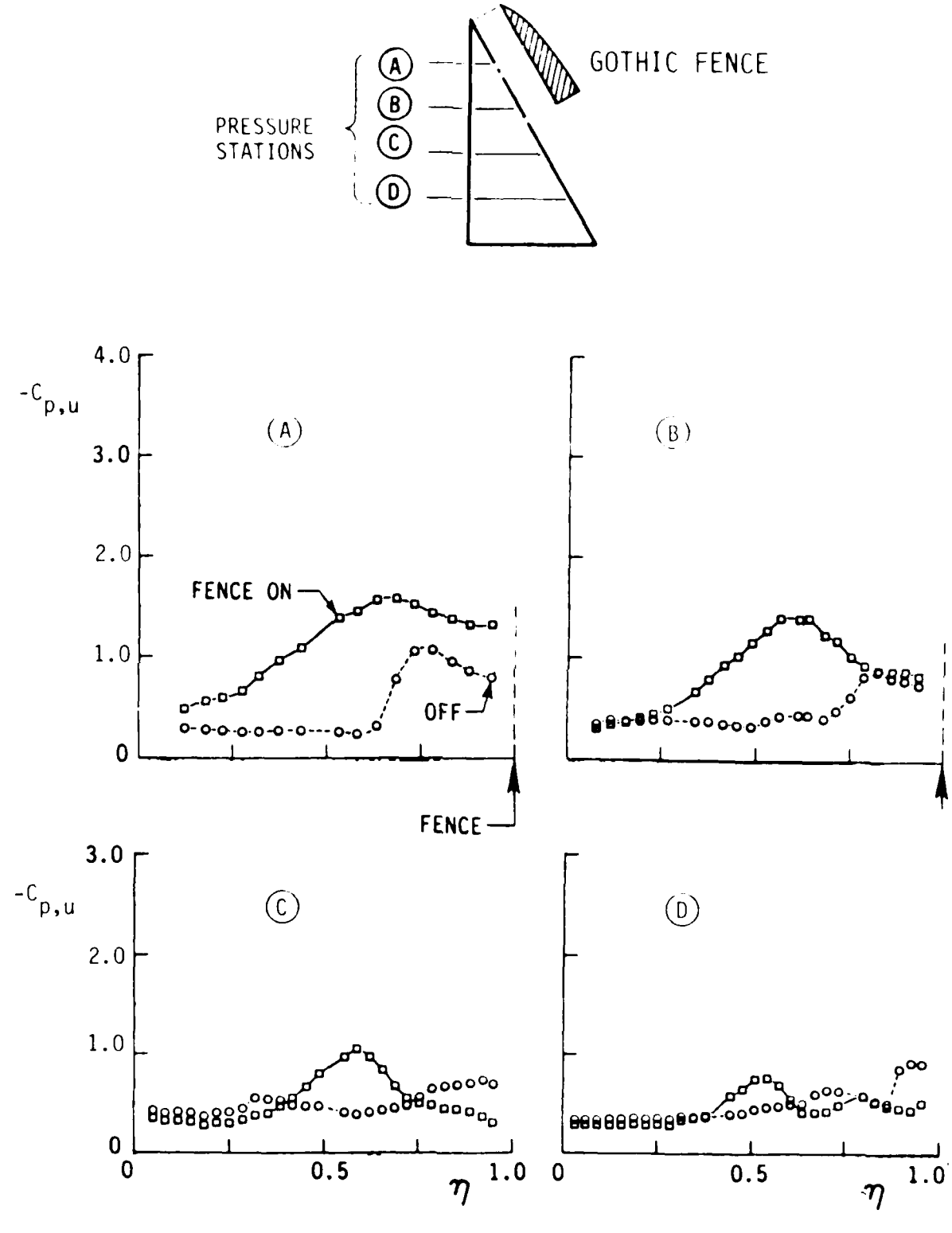

Fig. 15. Spanwise distributions of upper-surface pressure coefficient with and without gothic fences at 5 deg. angle of attack.

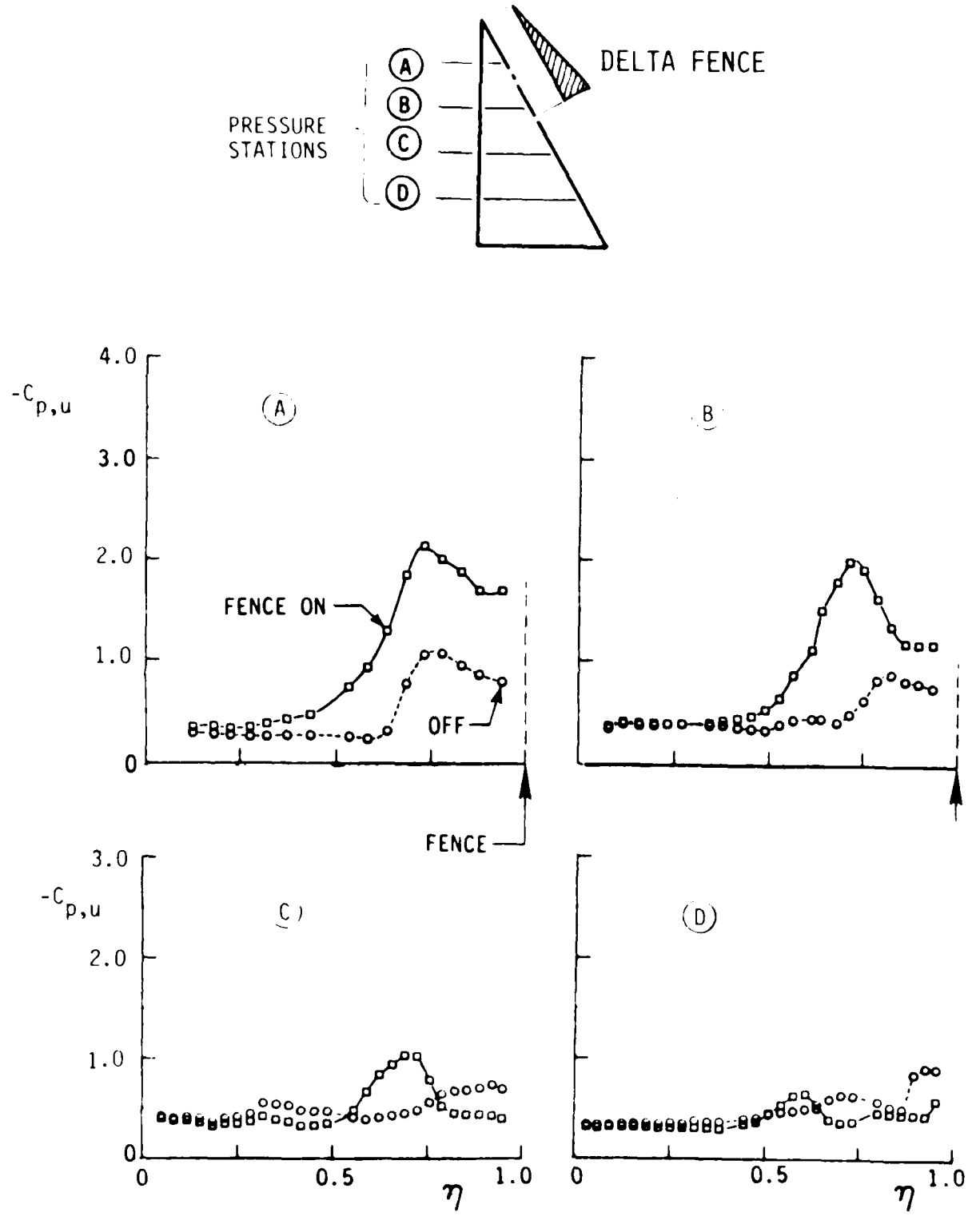

Fig. 16. Spanwise distributions of upper-surface pressure coefficient with and without delta fences at 5 deg. angle of attack.

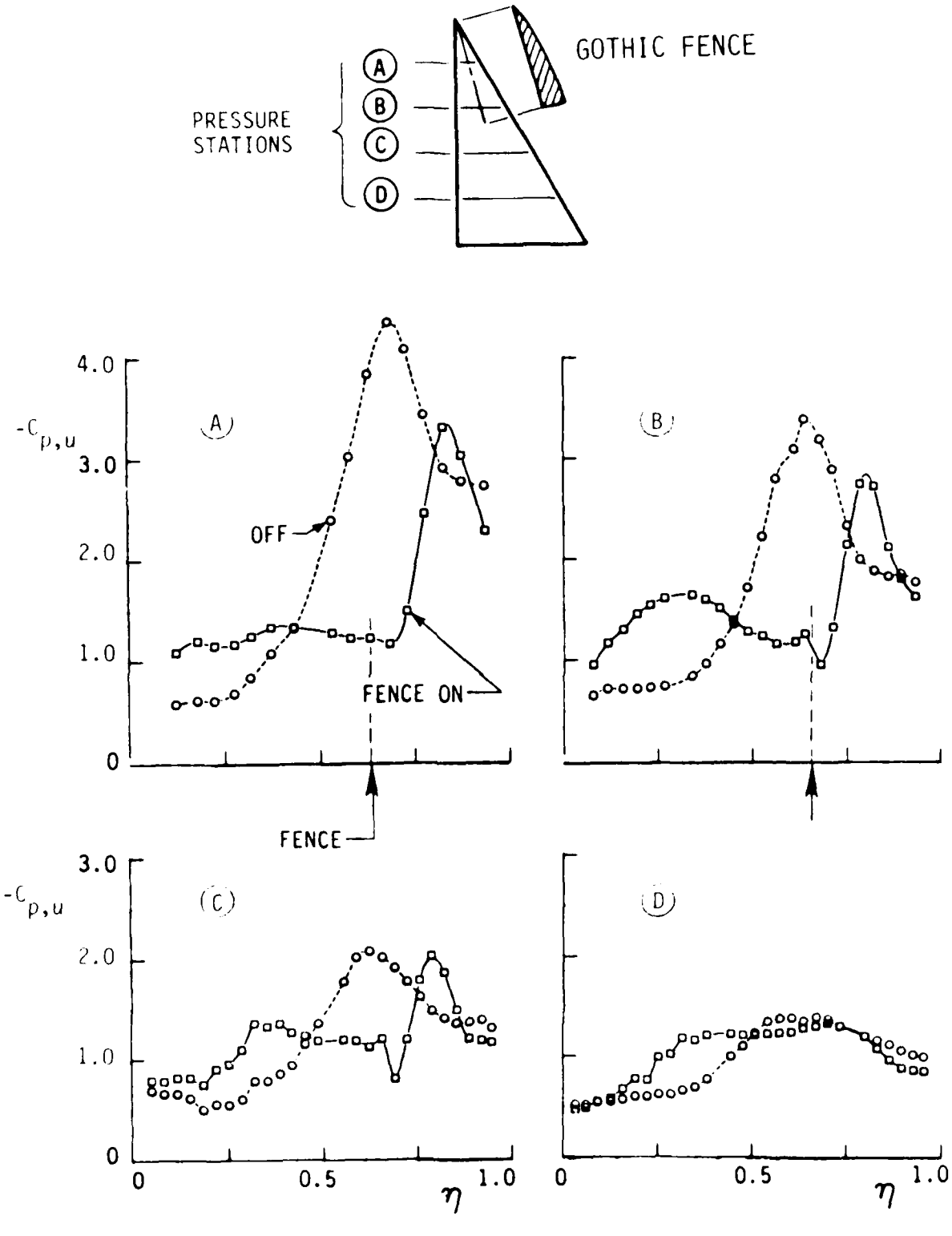

Fig. 17. Spanwise distributions of upper-surface pressure coefficient with and without fences at 20 deg. angle of attack.

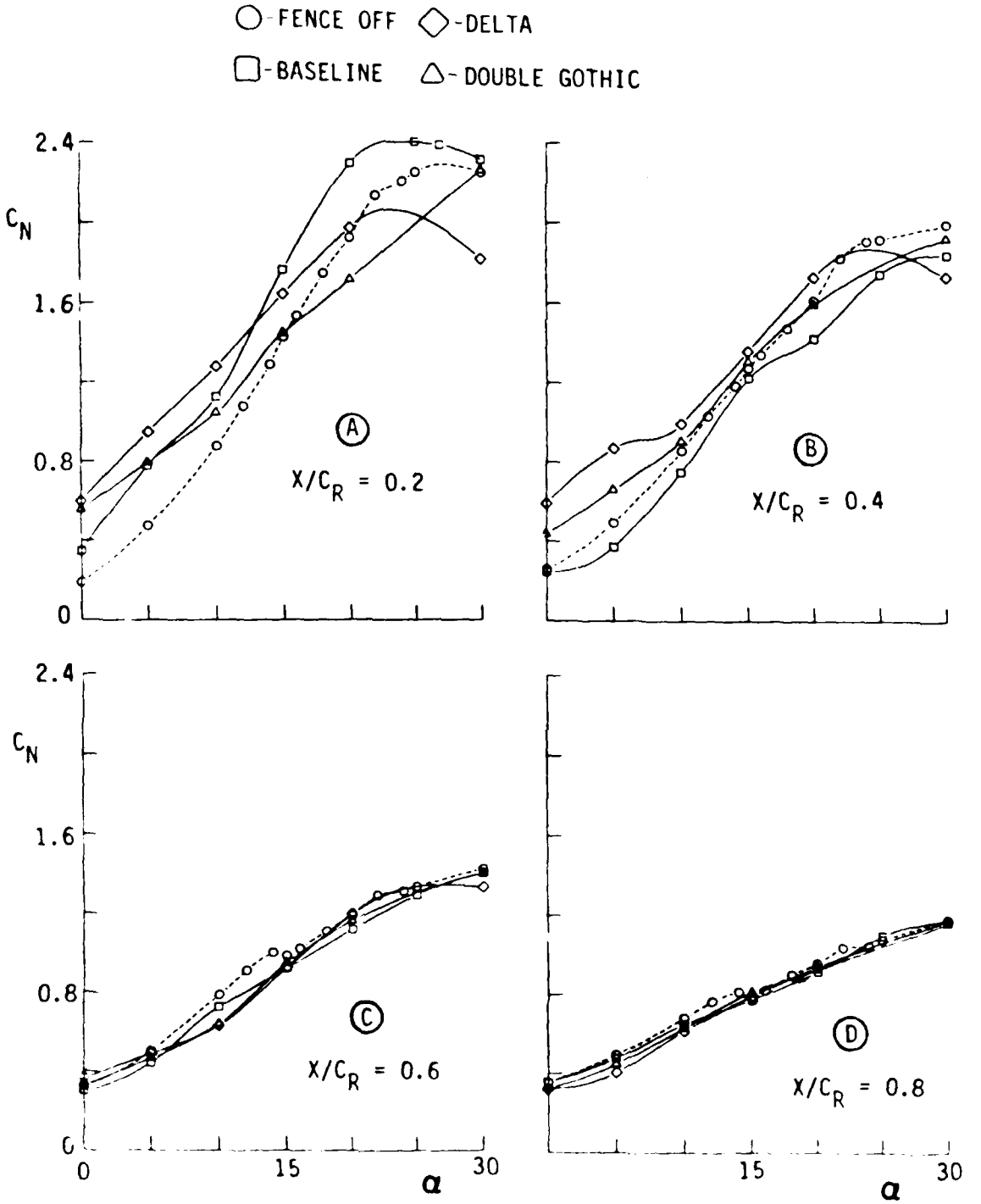

Fig. 18. Local normal force coefficient from upper-surface pressure integration with and without fences.

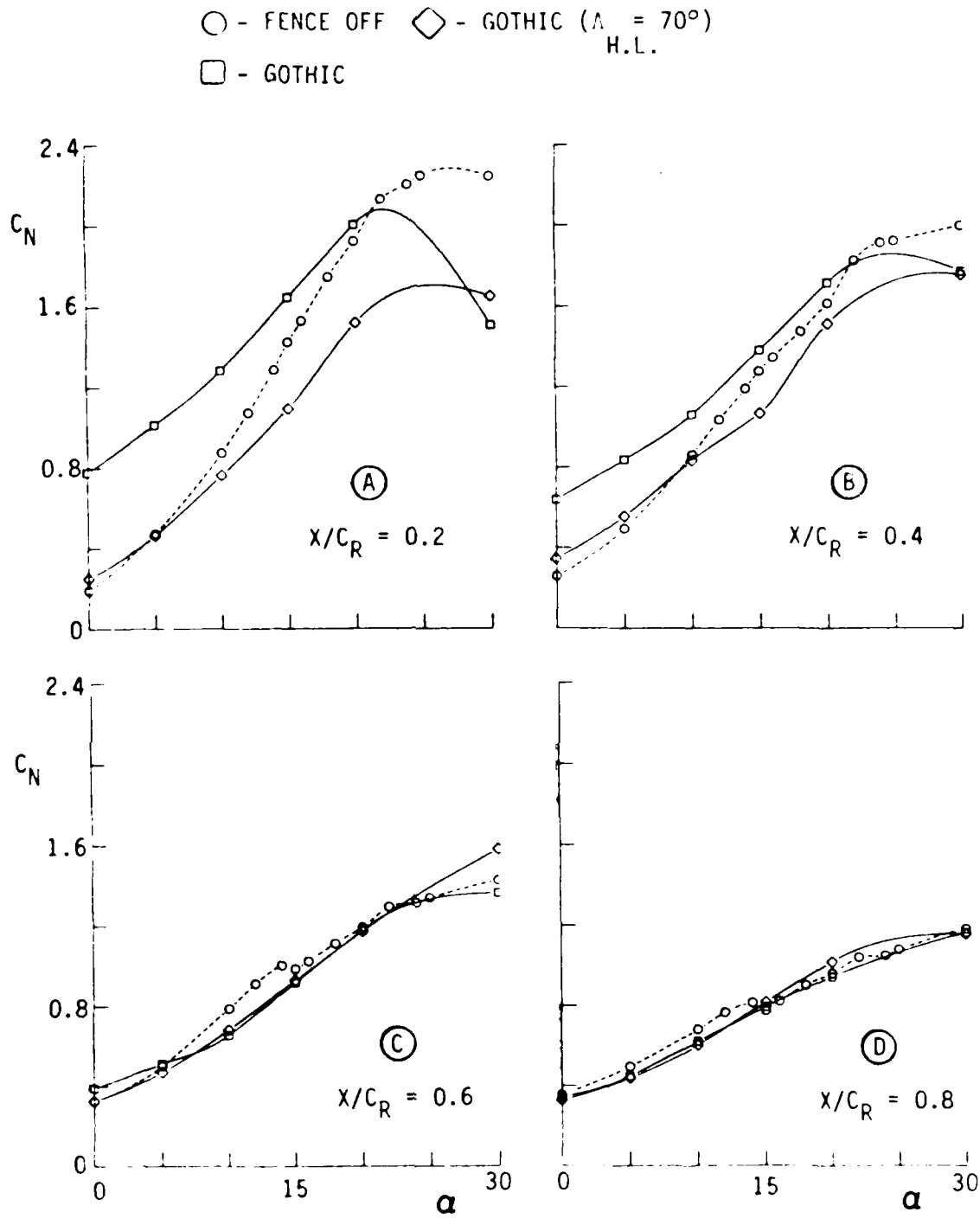

Fig. 19. Local normal force coefficient from upper-surface pressure integration showing effect of fence angle.

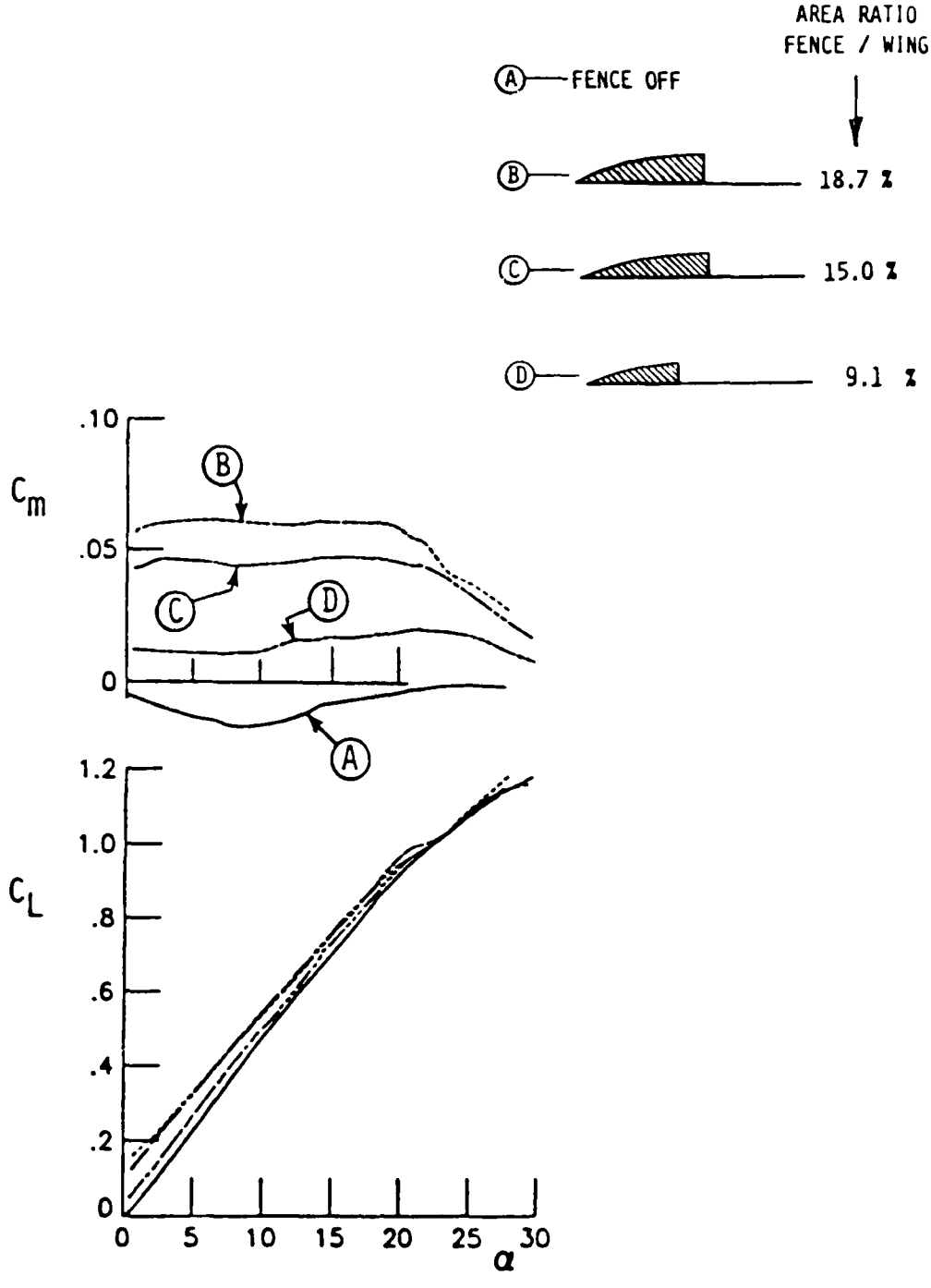

Fig. 20. Pitching moment and lift characteristics of gothic fences.

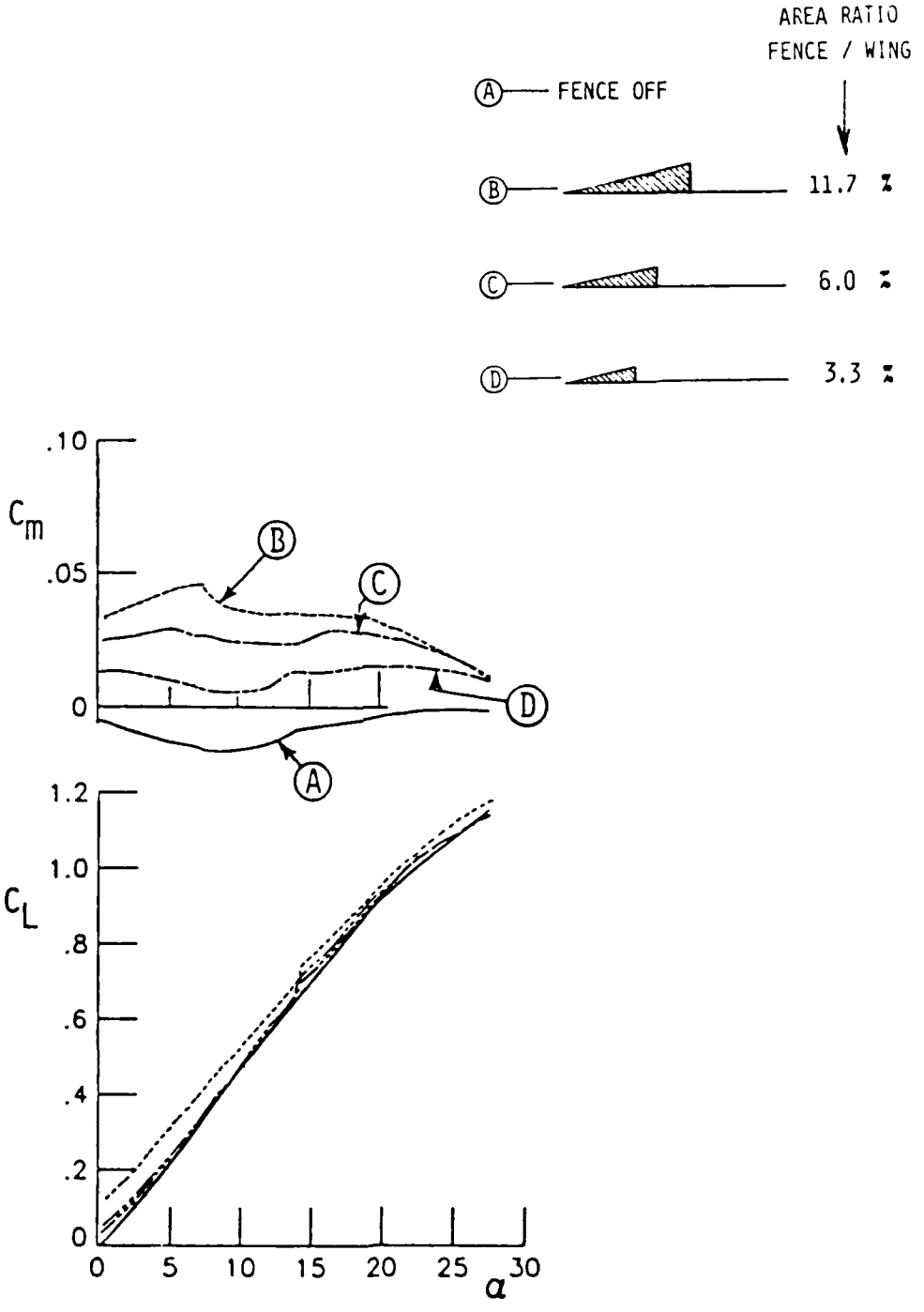

Fig. 21. Pitching moment and lift characteristics of delta fences.

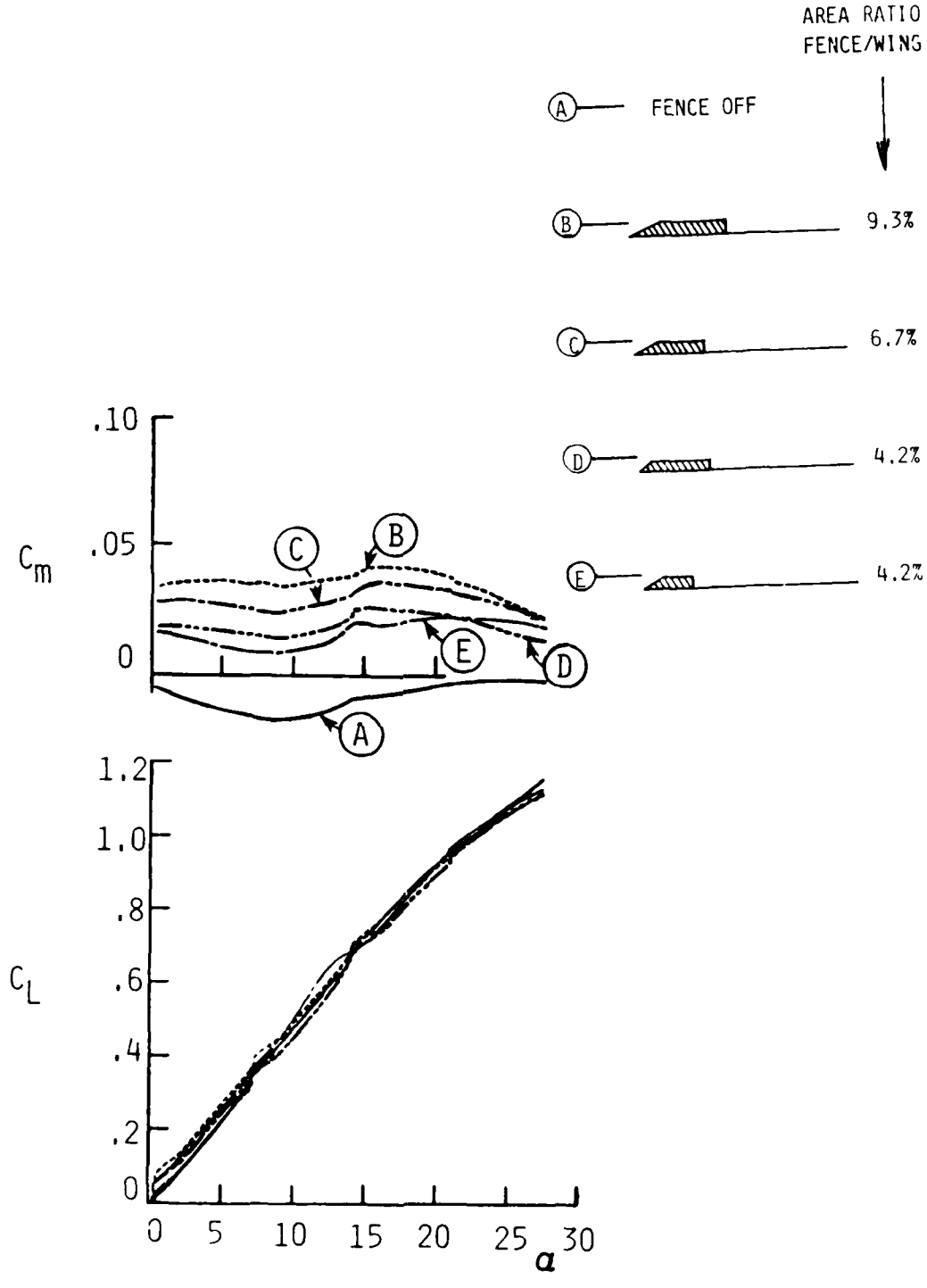

Fig. 22. Pitching moment and lift characteristics of cropped delta fences.

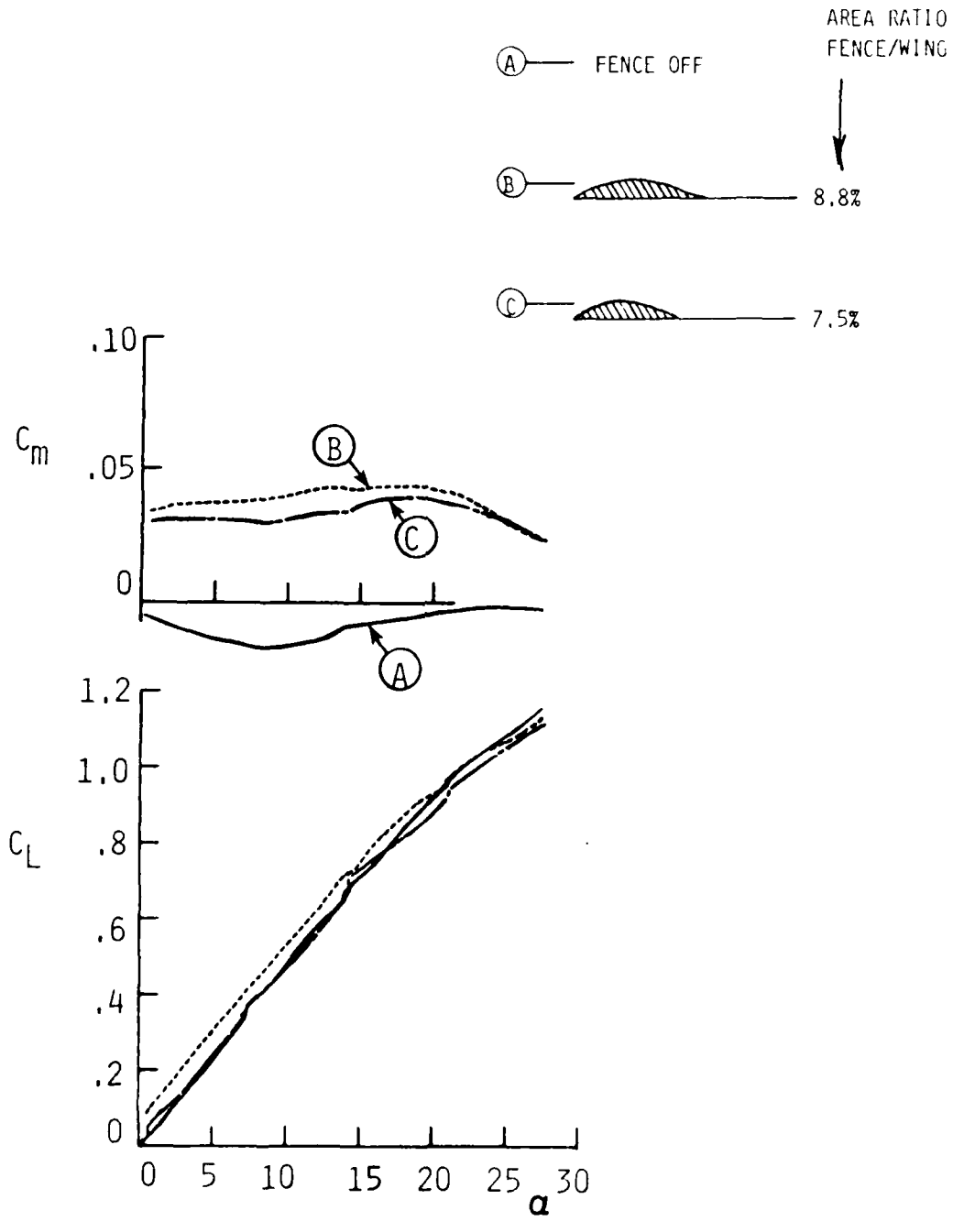

Fig. 23. Pitching moment and lift characteristics of double-gothic fences.

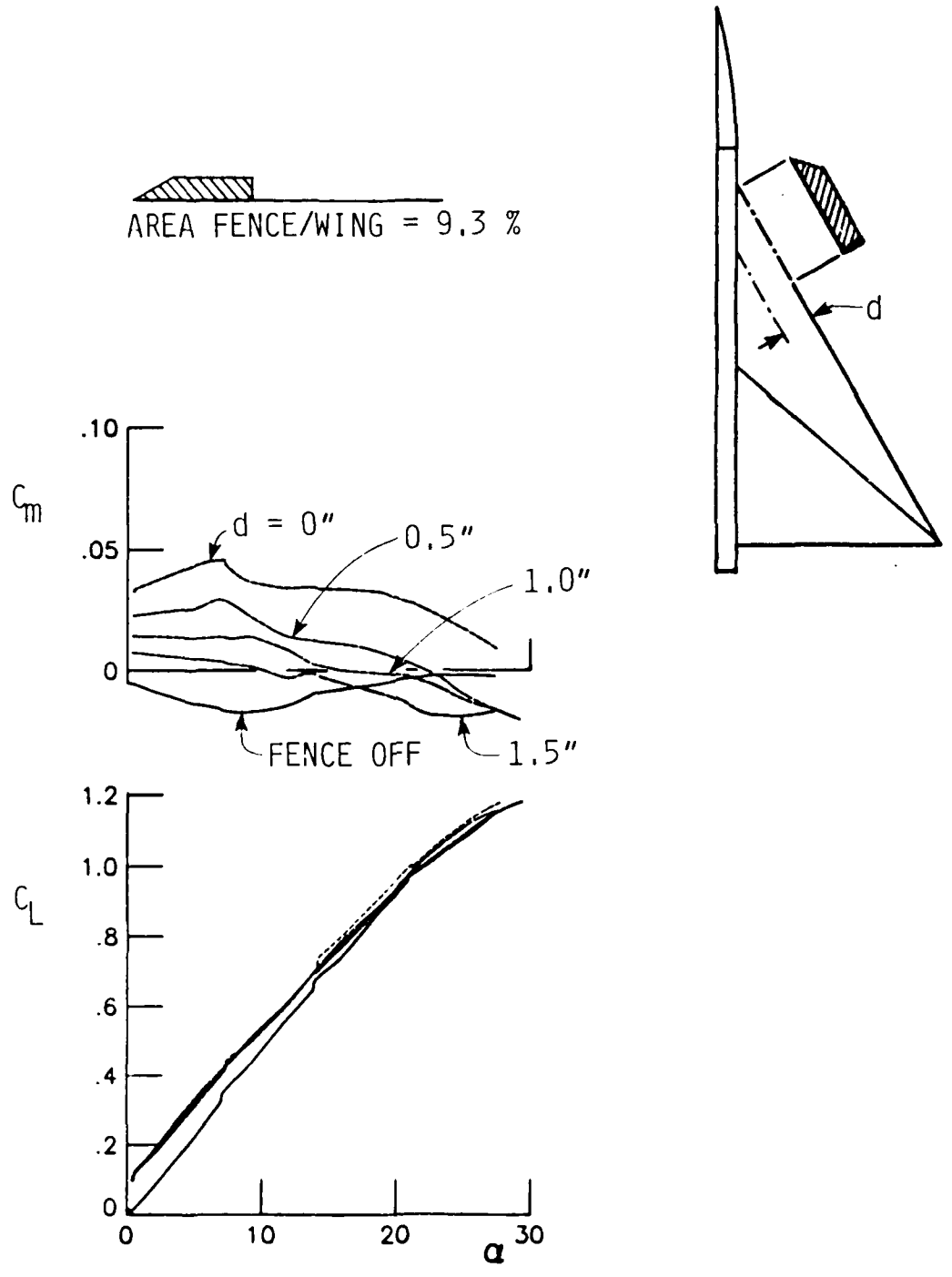

Fig. 24. Pitching moment and lift characteristics as a function of inboard shift of the fence hinge line.

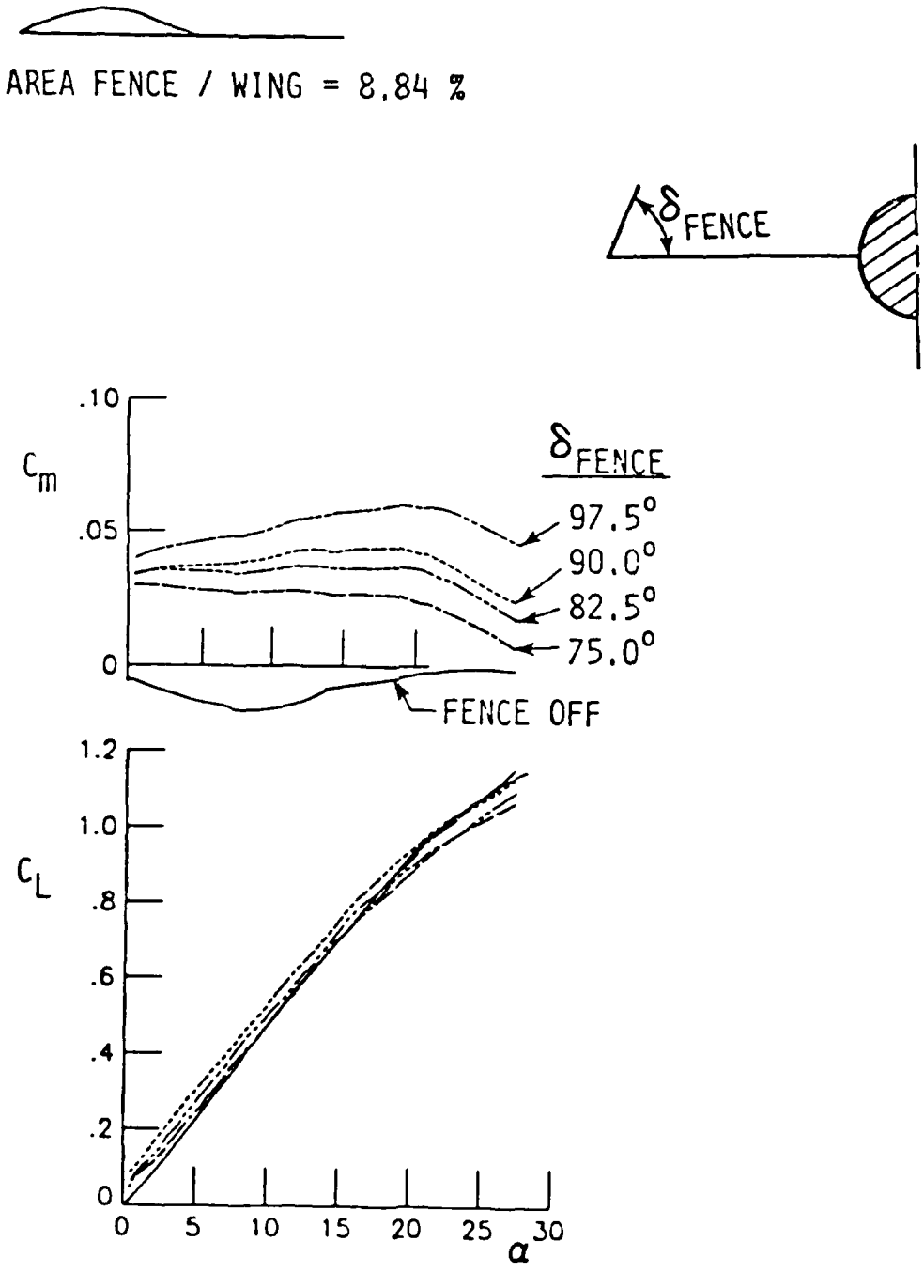

Fig. 25. Pitching moment and lift characteristics as a function of fence angle.

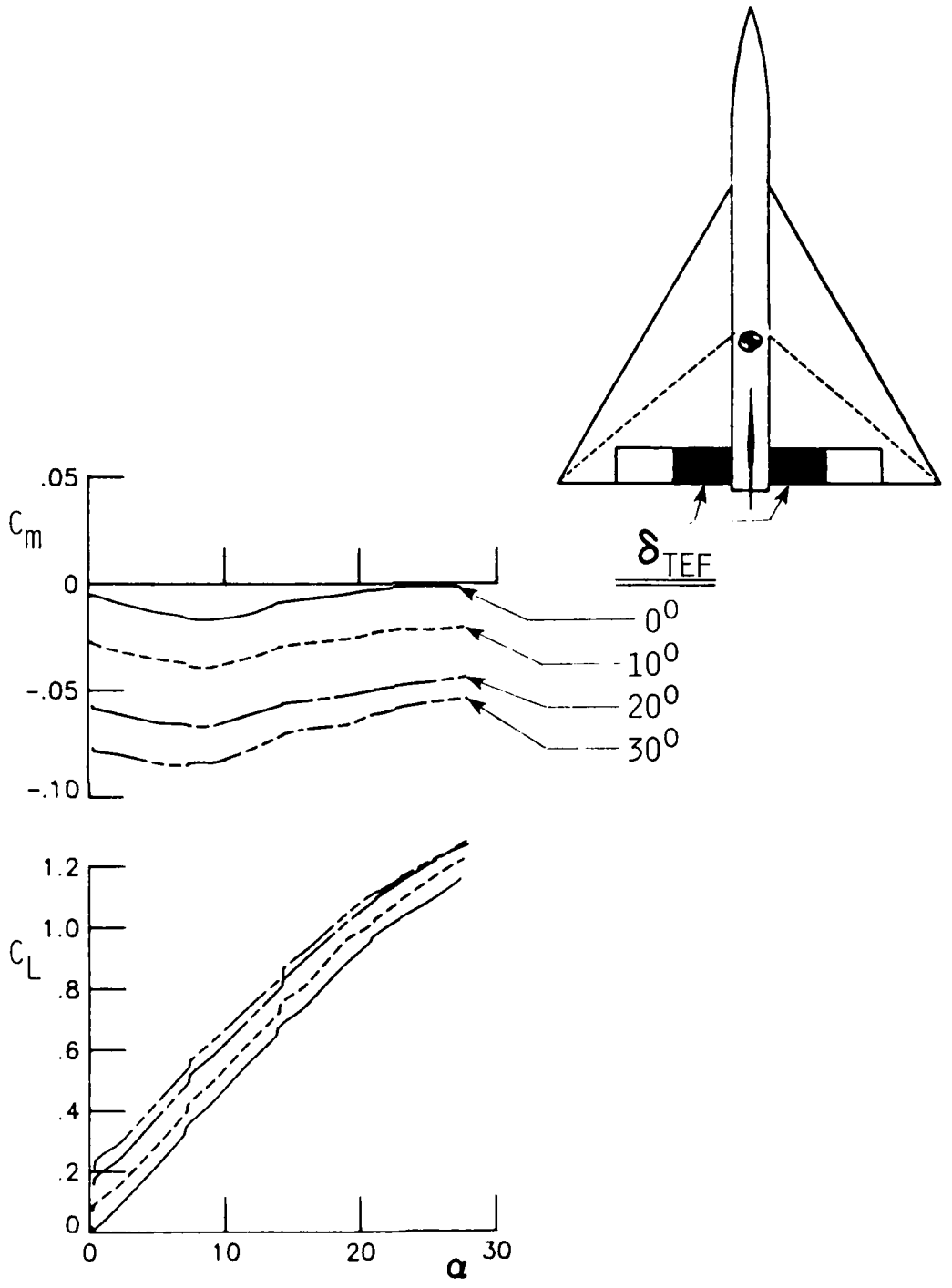

Fig. 26. Pitching moment and lift characteristics with various trailing edge flap deflection angles.

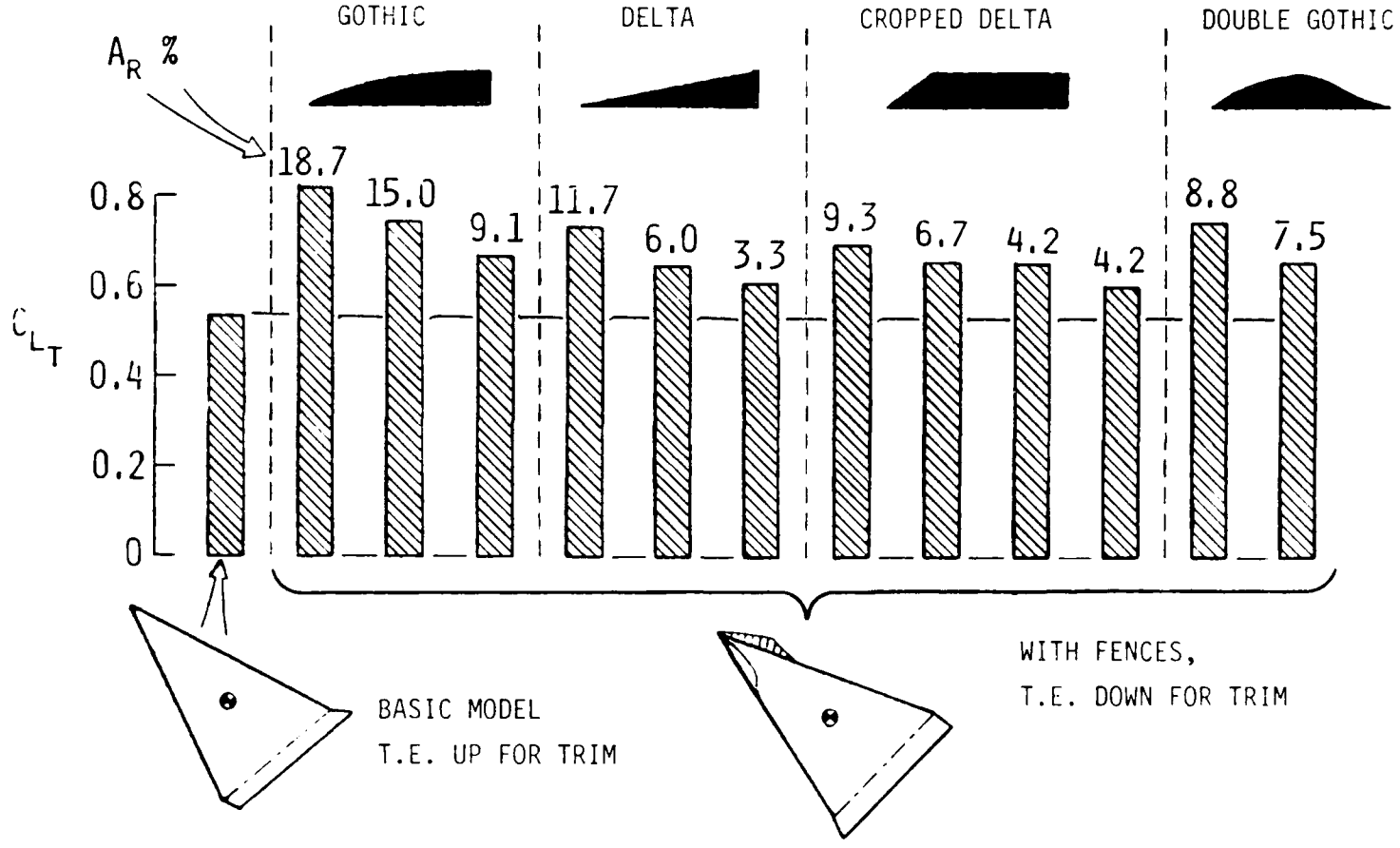

Fig. 27. Comparison of trimmed lift coefficient at 12 degrees angle of attack using different apex fences.

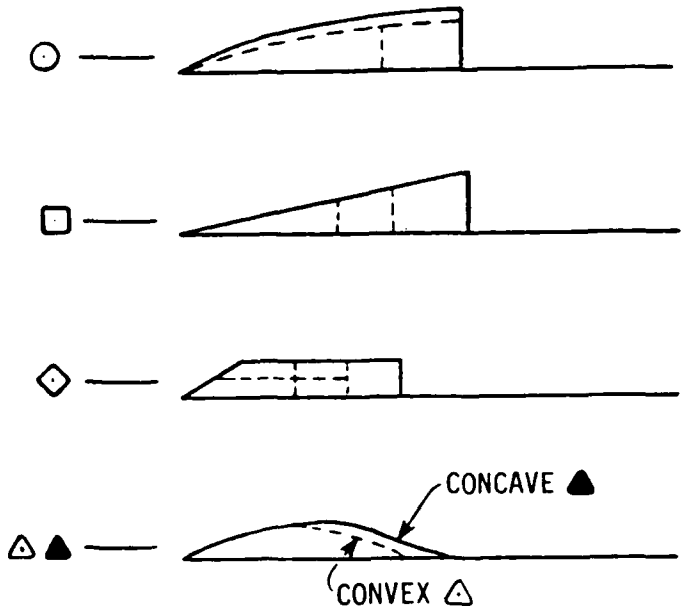

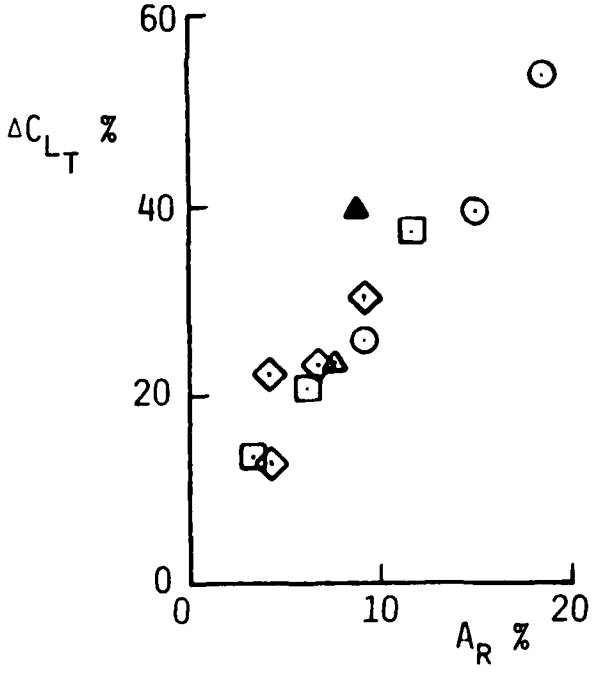

Fig. 28. Correlation of trimmed lift increment at α = 12 deg. with apex fence area ratio.

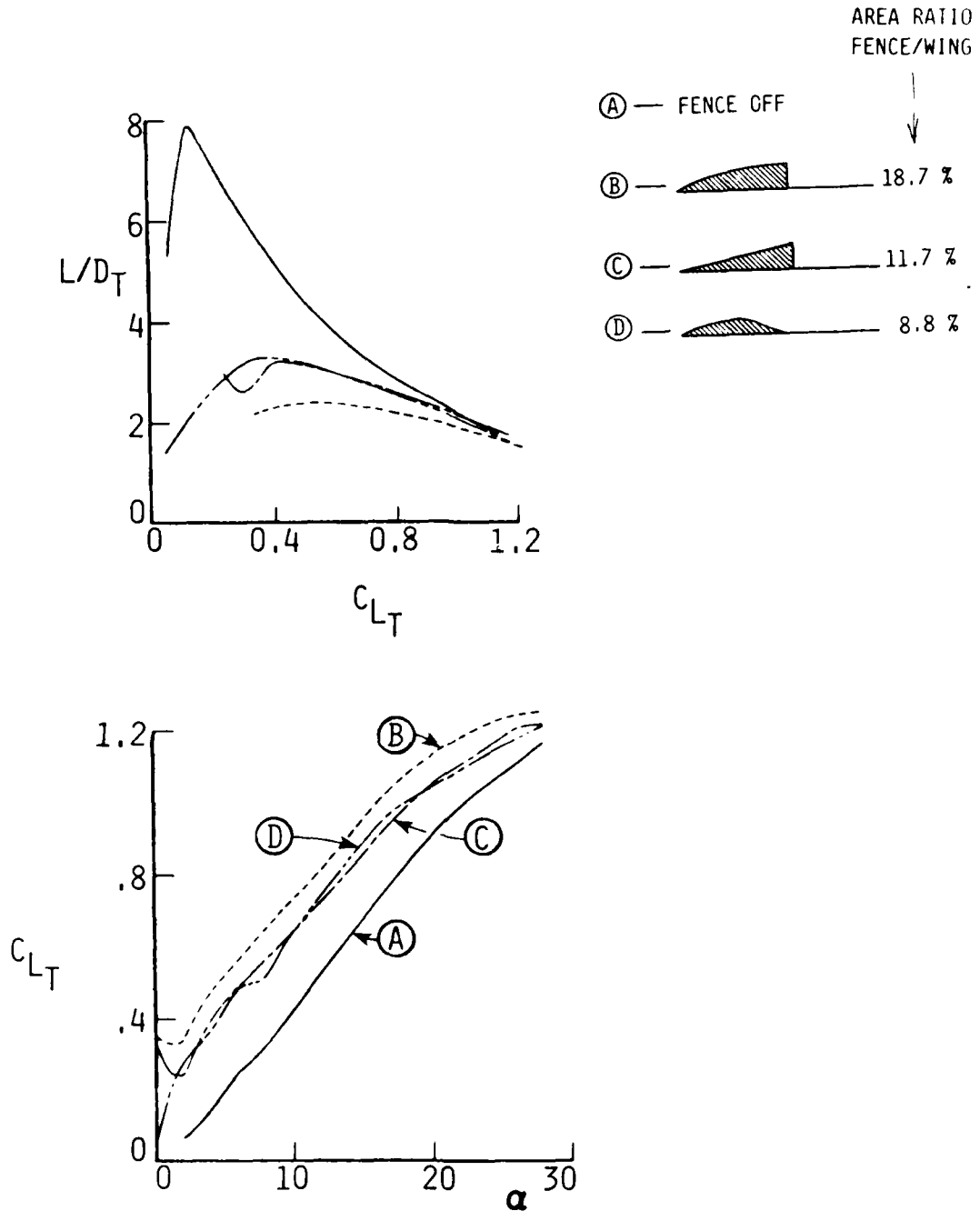

Fig. 29. Lift/drag ratio and trimmed lift characteristics with and without apex fences.

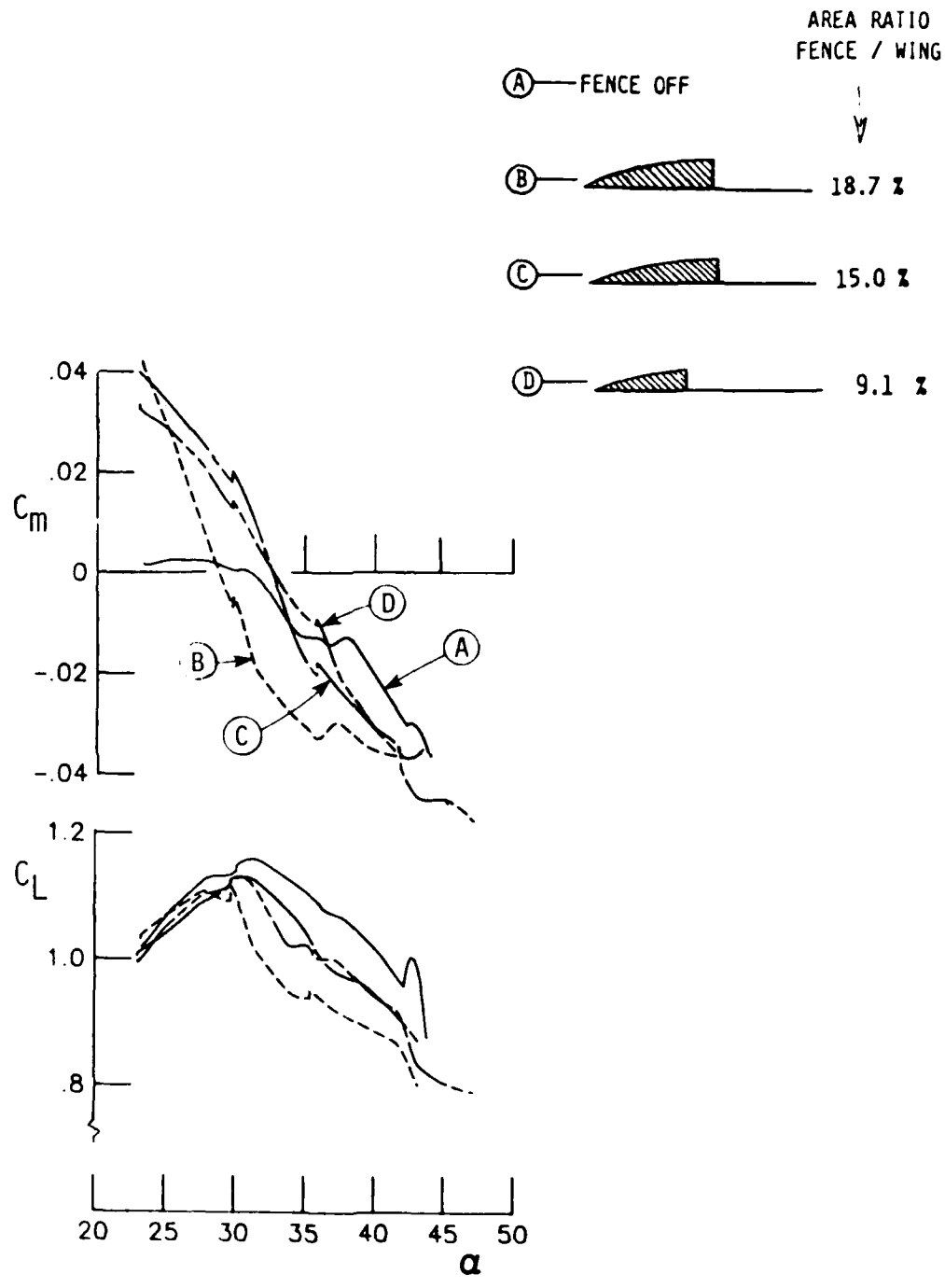

Fig. 30. High-angle-of-attack pitching moment and lift characteristics with various gothic fences.

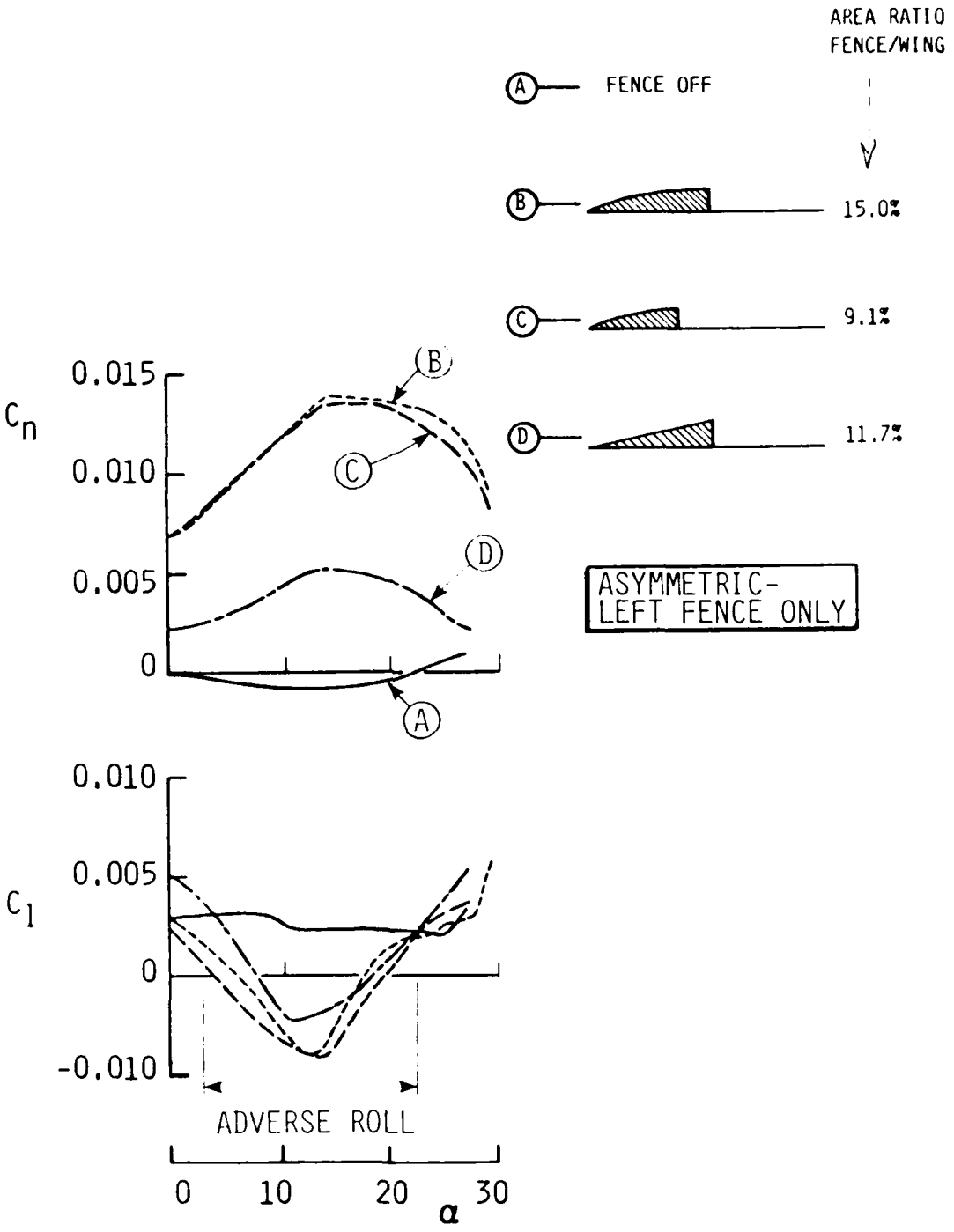

Fig. 31. Asymmetric fence effects on rolling and yawing moment characteristics at zero sideslip.

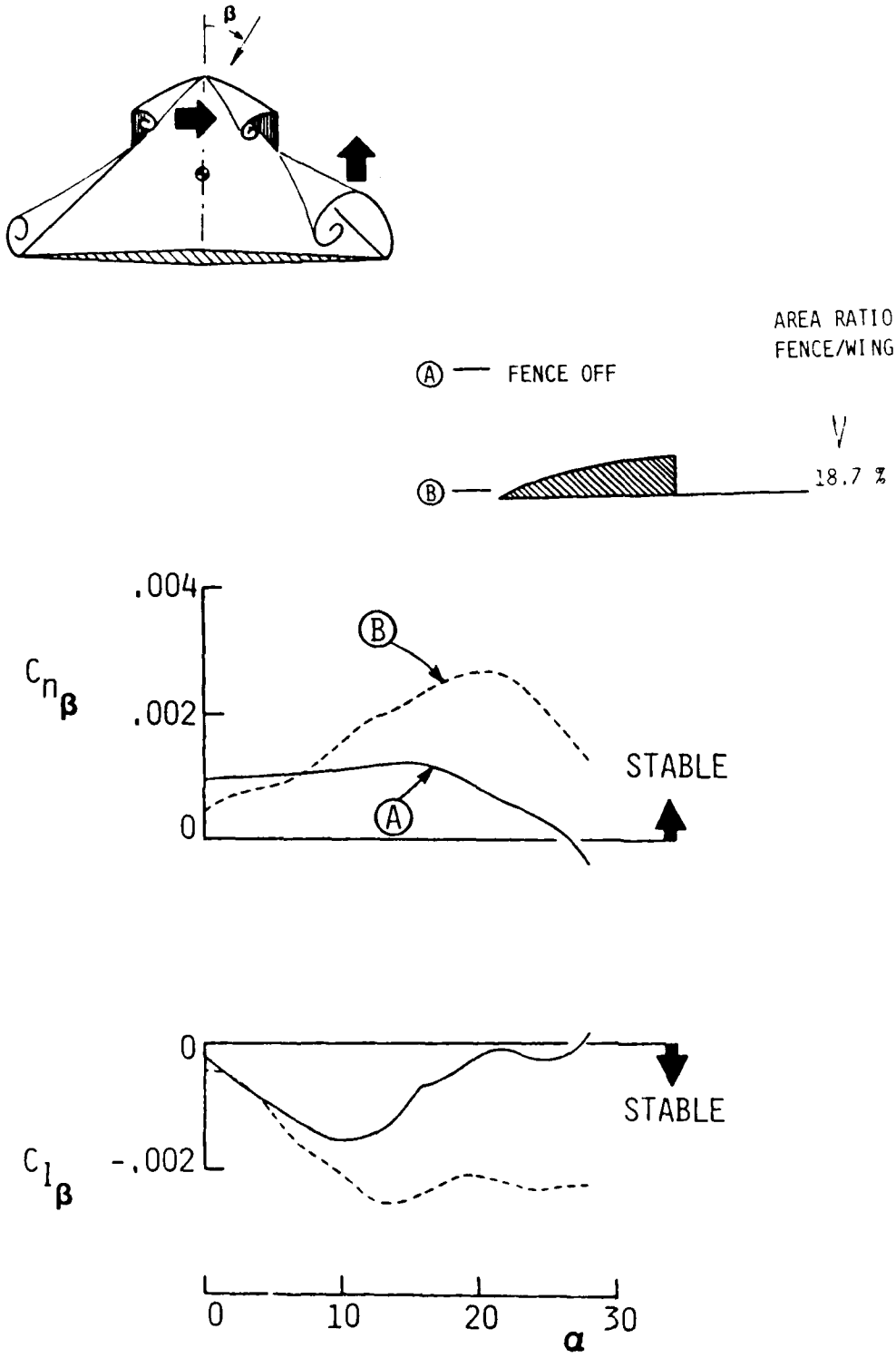

Fig. 32. Directional and lateral stability derivatives at 3 degrees sideslip angle with symmetric gothic fences.

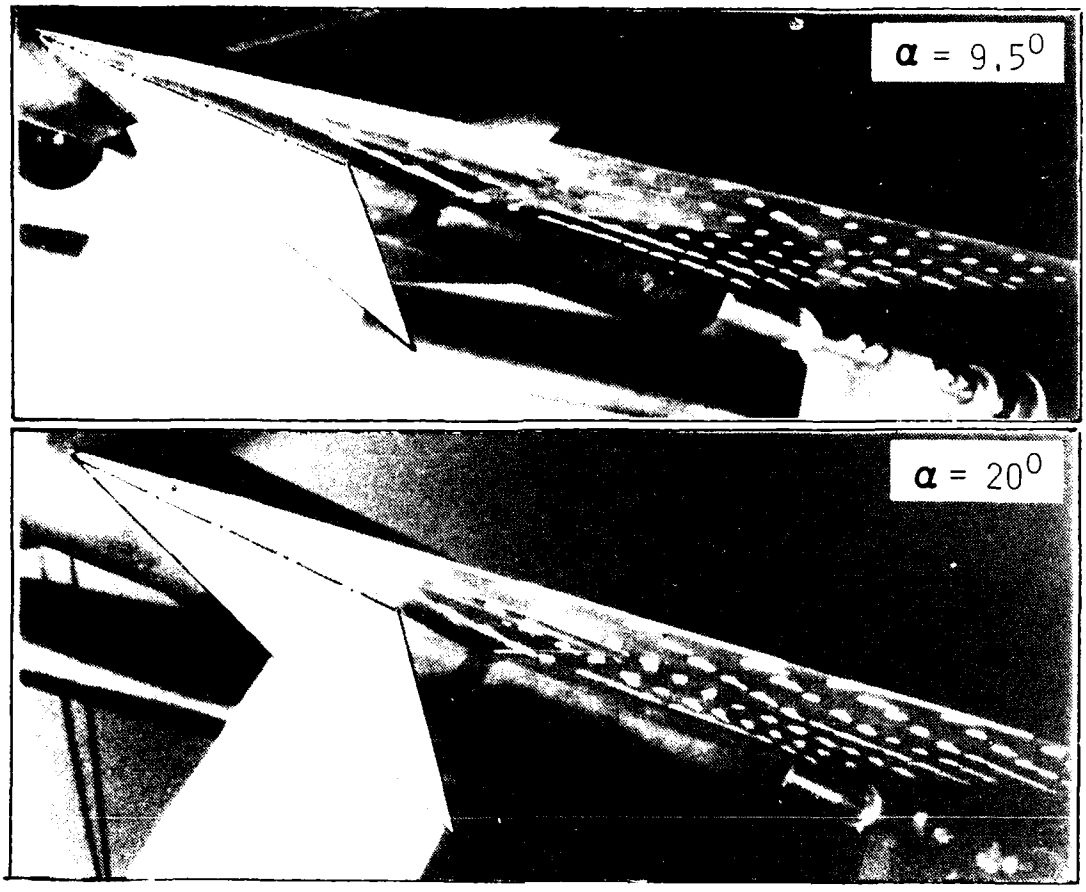

FLAP: CF-3/P1 $\delta_F = 60^0$

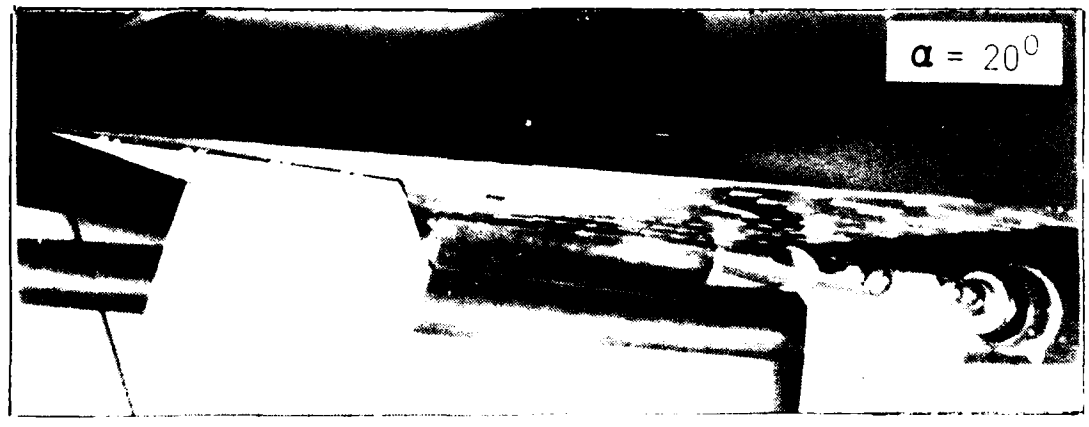

FLAP: CF-4/P2 $\delta_F = 60^0$

Fig. 33. Oil flow visualization on cavity flaps.

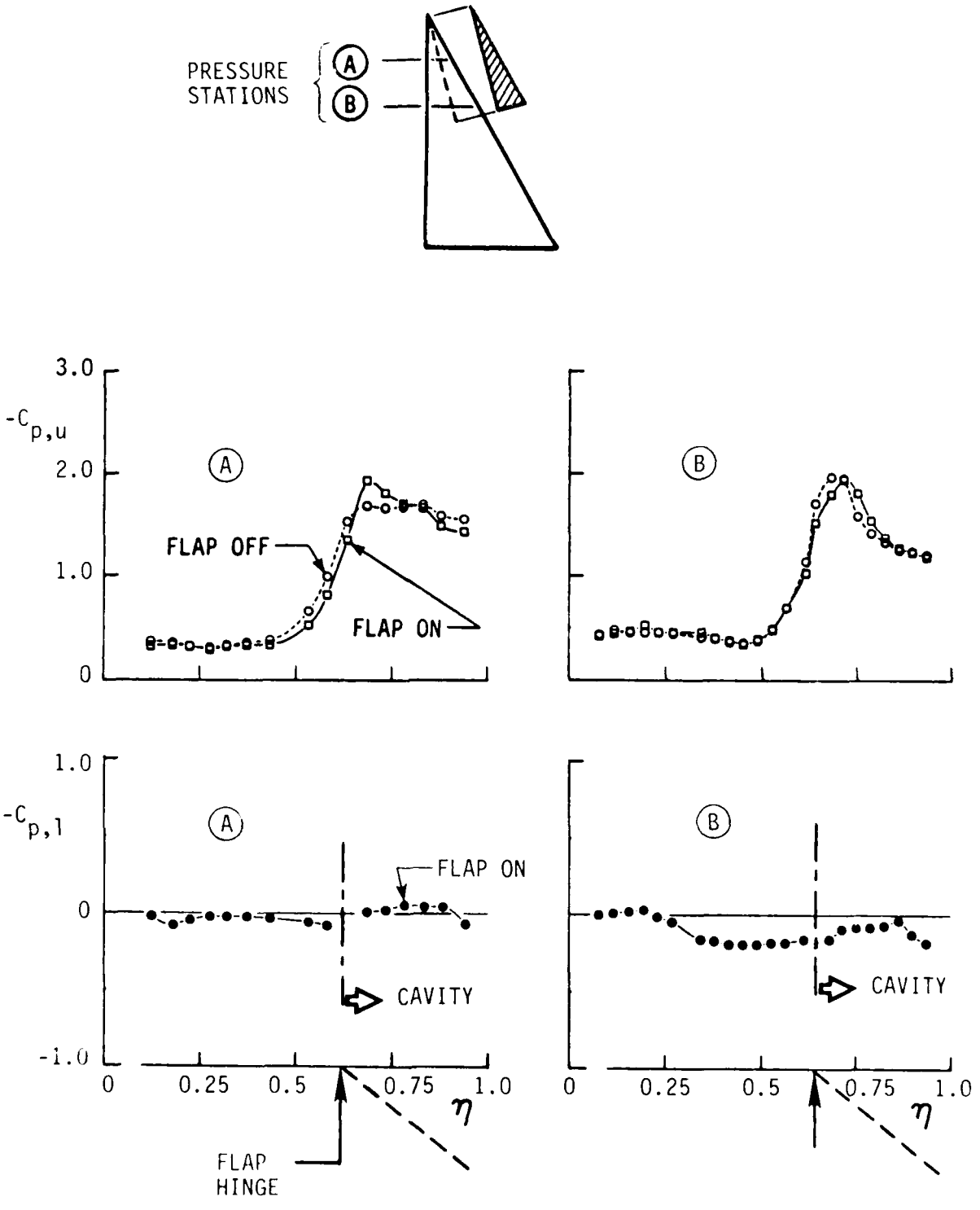

Fig. 34. Cavity flap effect on spanwise pressure distributions on wing upper and lower surfaces at α = 10 deg.

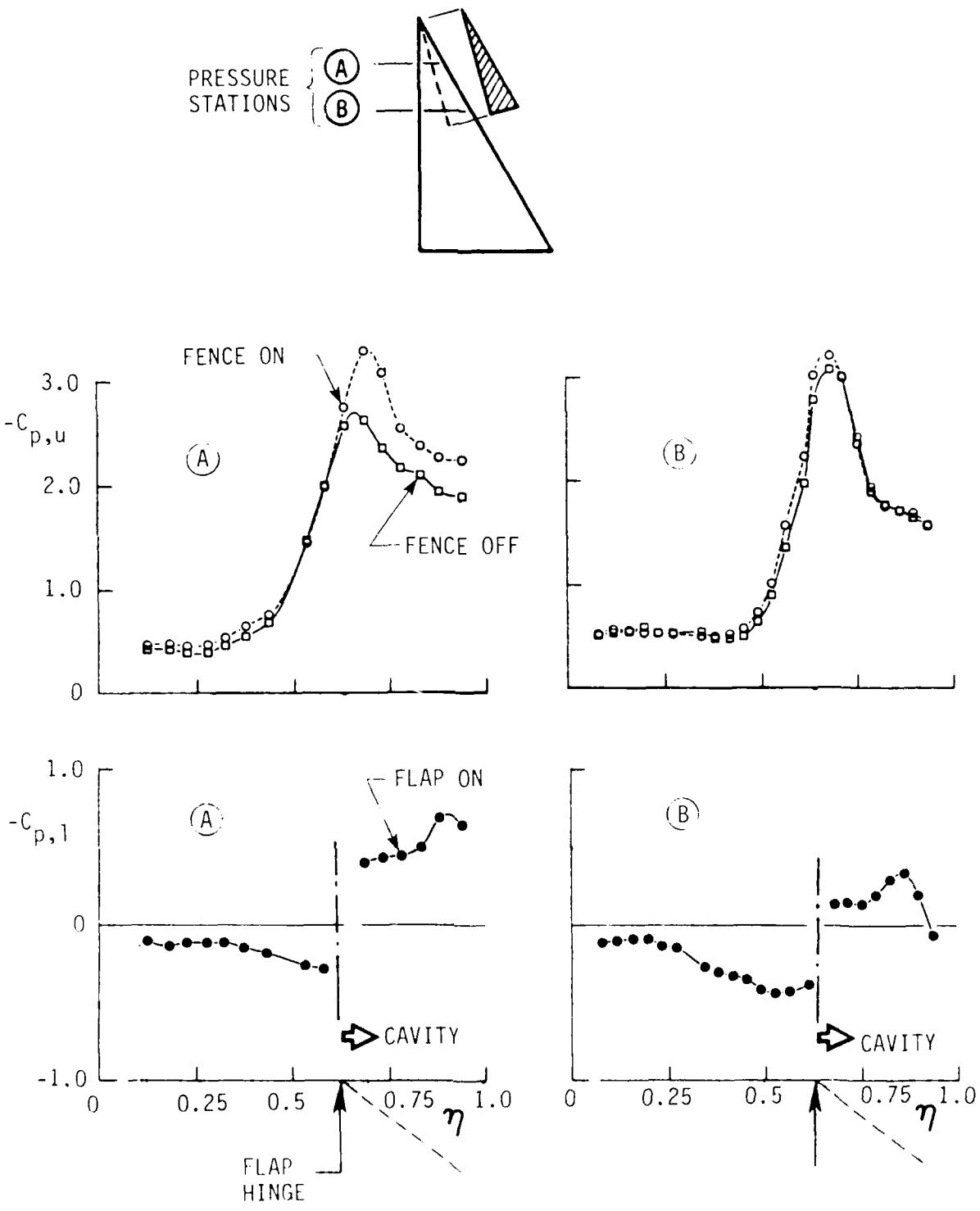

Fig. 35. Cavity flap effect on spanwise pressure distributions on wing upper and lower surface at α = 15 deg.

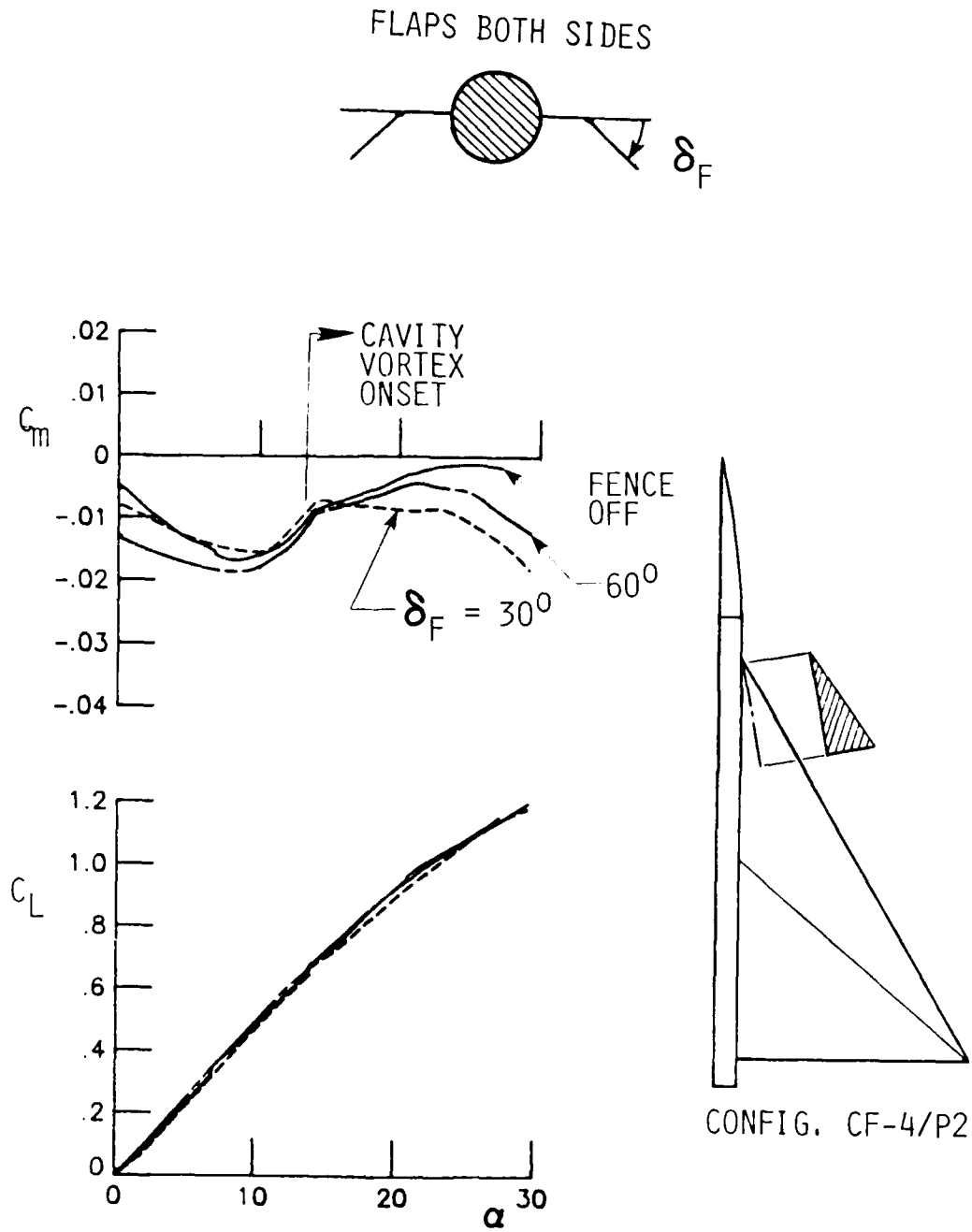

Fig. 36. Cavity flap effect on pitching moment and lift characteristics in 'low' angle-of-attack range.

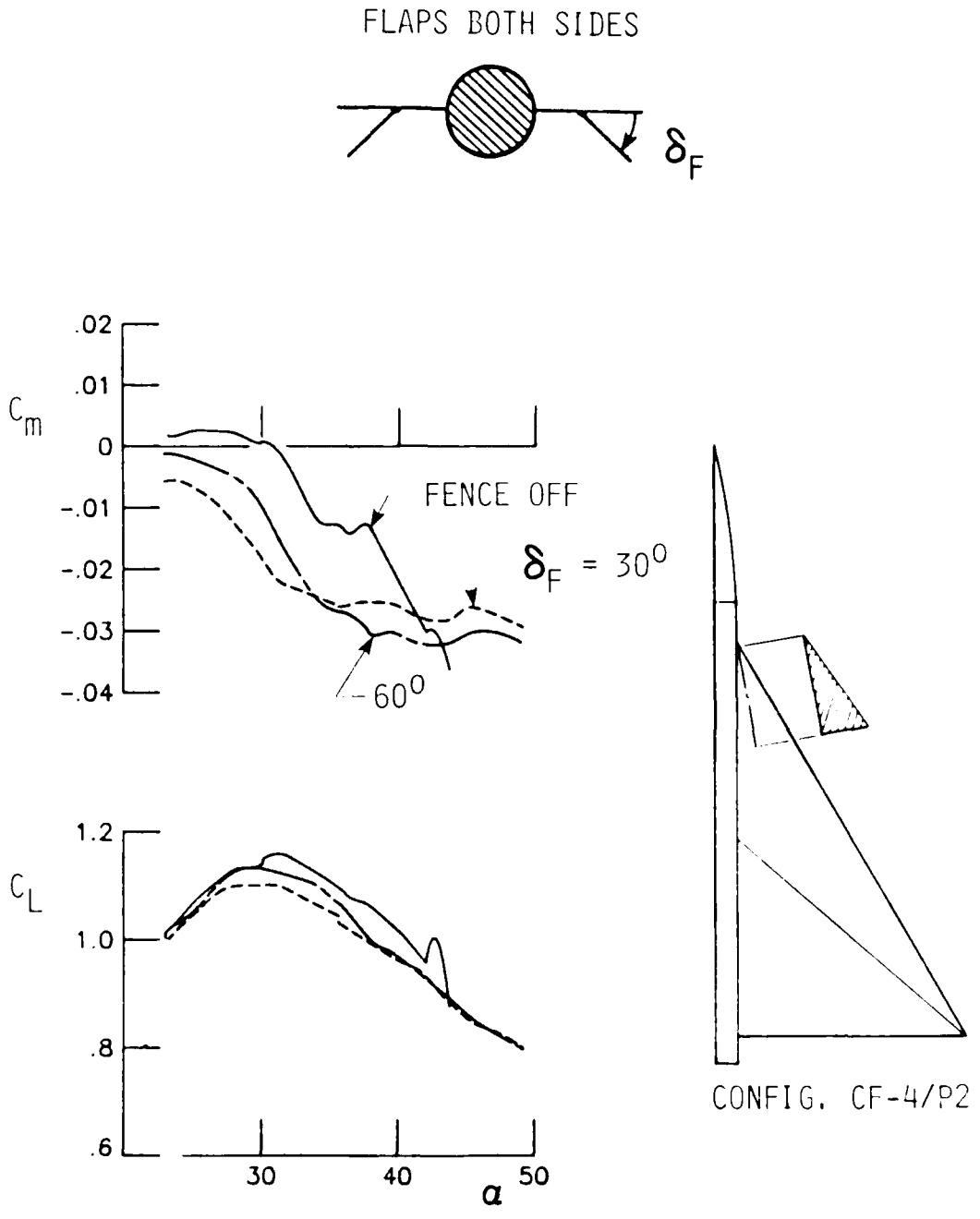

Fig. 37. Cavity flap effect on pitching moment and lift characteristics in 'high' angle-of-attack range.

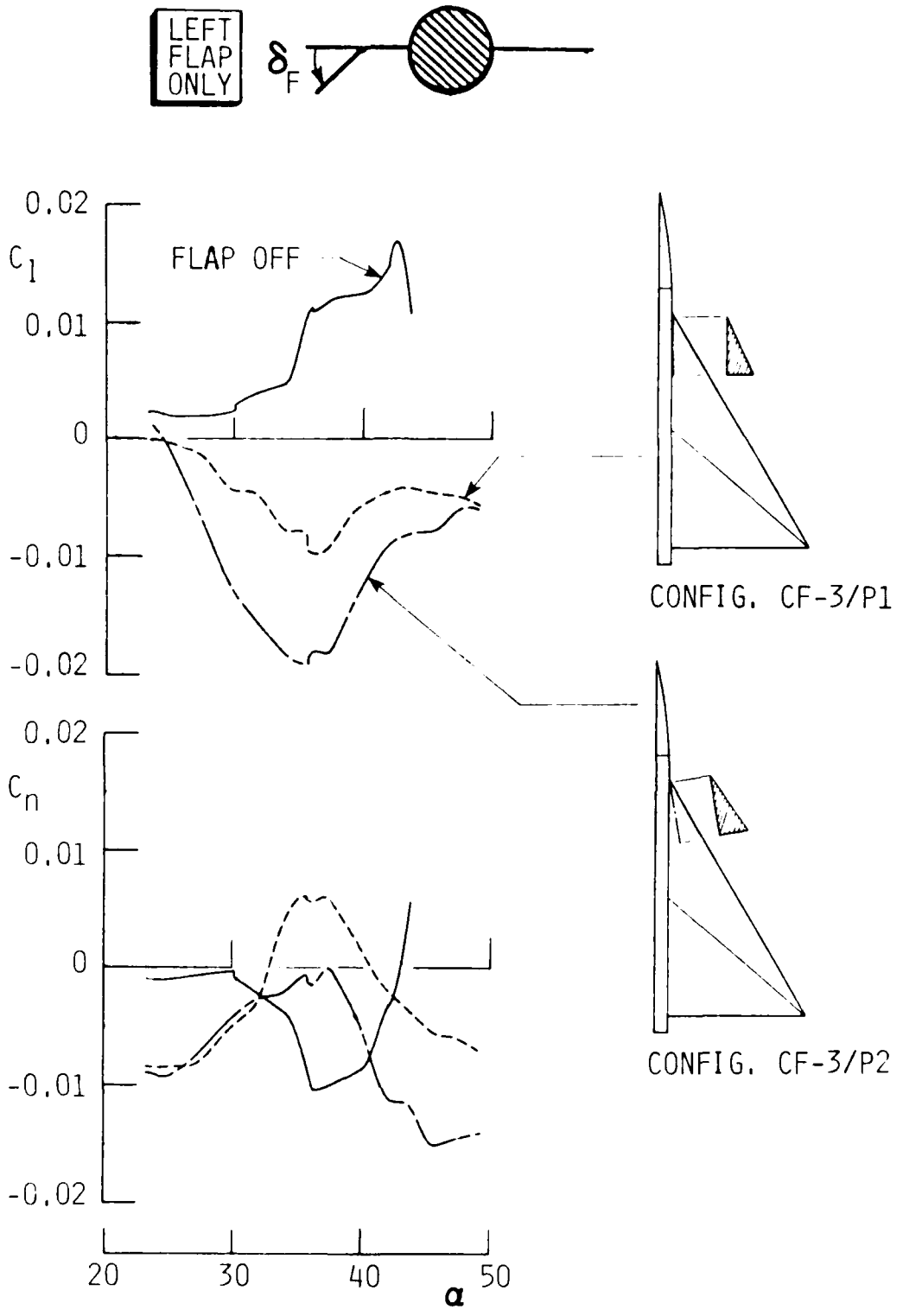

Fig. 38. Asymmetric 60 deg. deflected cavity flap effect on rolling and yawing moment characteristics in 'high' angle-of-attack range.

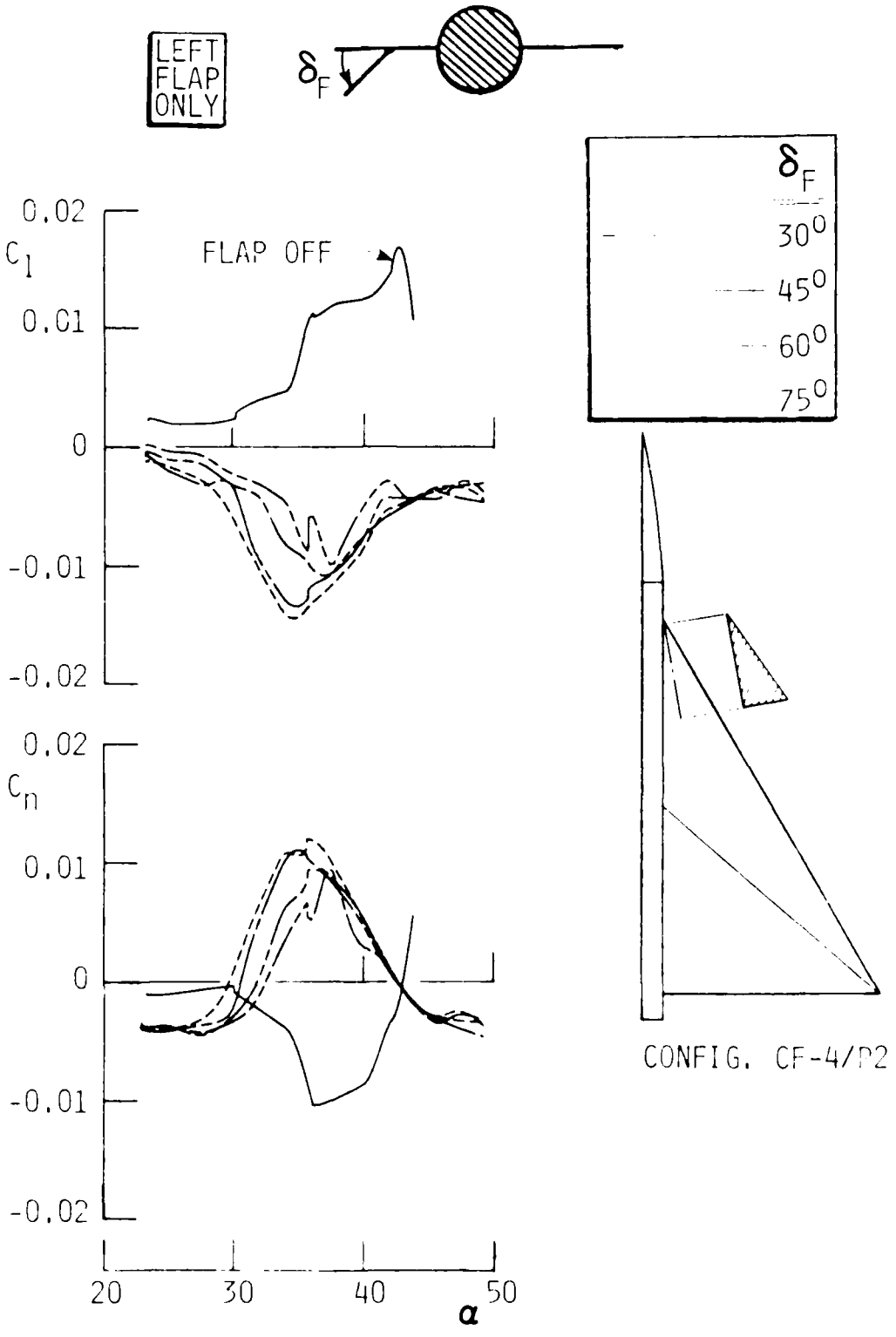

Fig. 39. Asymmetric cavity flap angle effect on rolling and yawing moment characteristics in the 'high' angle-of-attack range.

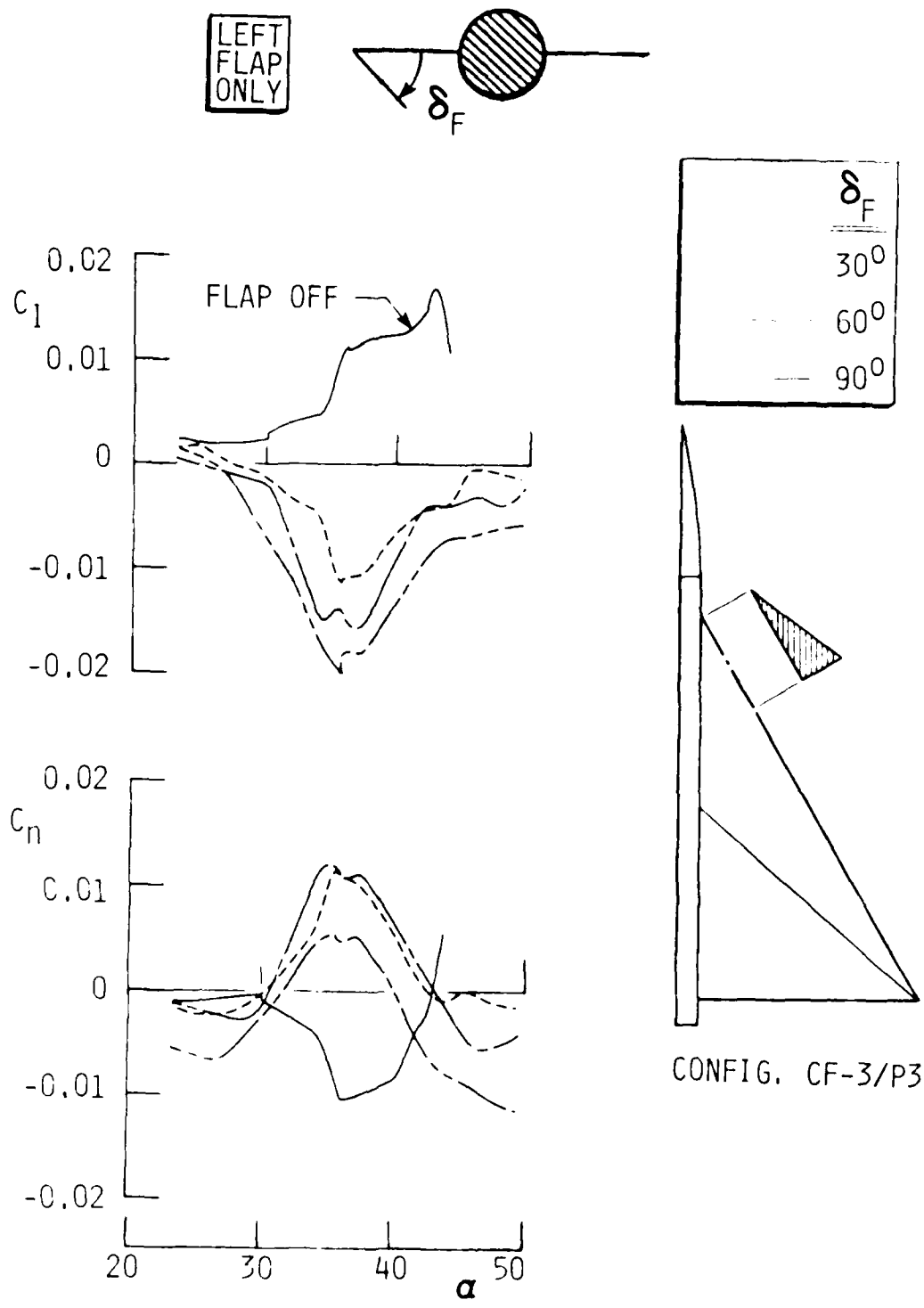

Fig. 40. Asymmetric, leading-edge hinged, cavity flap angle effect on rolling and yawing moment characteristics in the 'high' angle-of-attack range.

U.S Government Printing Office 1987 748 061 60985

END

8-87

DTIC